Adaptive mesh refinement, p-adaptivity, and sub-cell discontinuity resolution for high-order discretizations in engineering problems

John Ekaterinaris

Embry-Riddle Aeronautical University

Daytona Beach FL

ERAU

9th Ankara International Aerospace Congress
September 20 – 22, 2017 METU, Ankara Turkey

ERAU

Outline of the Presentation

- Motivation and Objectives
- Numerical Method
- The dissipative filter
- Results for model problems
- Outlook and future work

A discontinuous Galerkin approach for high-resolution simulations of three-dimensional flows, *Computer Methods in Applied Mechanic and Engineering* (2016) Vol. 299, pp. 254-282.

A nonlinear filter for high order discontinuous Galerkin discretizations with discontinuity resolution within the cell, *Journal of Computational Physics*, (2016), Vol. 326: pp. 234-257.

A p-adaptive method for electromagnetic wave propagation, *J Numer Meth Engng*. 2017; 1–25. https://doi.org/10.1002/nme.5577

Motivation and Objectives

- To develop a unified efficient approach for both smooth flows including complex flow features and discontinuity capturing when using higher-order (P2 or higher) DG discretizations in three-dimensional unstructured meshes

- To allow capabilities of using large cells and high order accuracy both at discontinuities (with sub-cell discontinuity resolution) and away from them in order to resolve smooth but complex flow features.

- To advance implicitly in time (using Newton-Krylov or space time FE methods) the full coupled system for compressible viscous flows, chemically reactive flows, and ionized gas plasma flows

- To apply and demonstrate potential benefits from dynamic h/p refinement for time dependent complex three dimensional flow problems.

ERAU

DG discretization

$$\frac{\partial U}{\partial t} + div\,\bar{\bar{Q}} = S$$

- Weak form of the system

$$\int_{\Omega} \Phi \frac{\partial \boldsymbol{U}}{\partial t}\, d\Omega = \int_{\Omega} \nabla\Phi \cdot \boldsymbol{Q}(\boldsymbol{U},\nabla \boldsymbol{U})\, d\Omega - \int_{\partial\Omega} \Phi \boldsymbol{Q}(\boldsymbol{U},\nabla \boldsymbol{U}) \cdot \boldsymbol{n}\, dA + \int_{\Omega} \Phi \cdot \boldsymbol{S}(\boldsymbol{U})\, d\Omega$$

- Use the same polynomial spaces for weighting and expansion functions

- The approximate solution is $\boldsymbol{U}_h = \sum_i c_i \Phi_i$, and the discrete weak form becomes

$$\mathrm{M}\frac{\partial \mathbf{c}}{\partial t} = \int_{K} \nabla\Phi_i \cdot \boldsymbol{Q}(\boldsymbol{U}_h,\nabla \boldsymbol{U}_h)\, dK - \int_{S_K} \Phi_i \widehat{\boldsymbol{Q}}(\boldsymbol{U}_h,\nabla \boldsymbol{U}_h) \cdot \boldsymbol{n}\, dS_K + \int_{K} \Phi_i \boldsymbol{S}(\boldsymbol{U}_h)\, dK$$

- Use the LLF or Roe's flux to evaluate the interface fluxes

LLF flux $$\widehat{\boldsymbol{Q}}(\boldsymbol{U}_h) = 0.5\left[\boldsymbol{Q}^{+}(\boldsymbol{U}_h)\cdot \boldsymbol{n} + \boldsymbol{Q}^{-}(\boldsymbol{U}_h)\cdot \boldsymbol{n} - \lambda_{\max}(\boldsymbol{U}_h^{-} - \boldsymbol{U}_h^{+})\right]$$

ERAU

DG discretization of the viscous terms

ERAU

- Define the auxiliary variable $\Theta = \nabla \mathbf{U}_f$ for the gradient of the state vector and discretize it in the same DG framework

$$\mathrm{M}\boldsymbol{c} = \int_{S_K} \Phi_i \widehat{\boldsymbol{U}}_h \cdot \boldsymbol{n} dS_K - \int_K \nabla \Phi_i \cdot \boldsymbol{U}_h dK$$

- Use the LDG or the BR2 scheme to evaluate the numerical fluxes
- For the current computations we used the LDG method
- For arbitrary three dimensional meshes the BR2 scheme is more suitable because it yields more narrow stencils strictly confined to the immediate neighbors of an element

The map from arbitrary prismatic and tetrahedral elements in physical space to the standard computational space cubical element

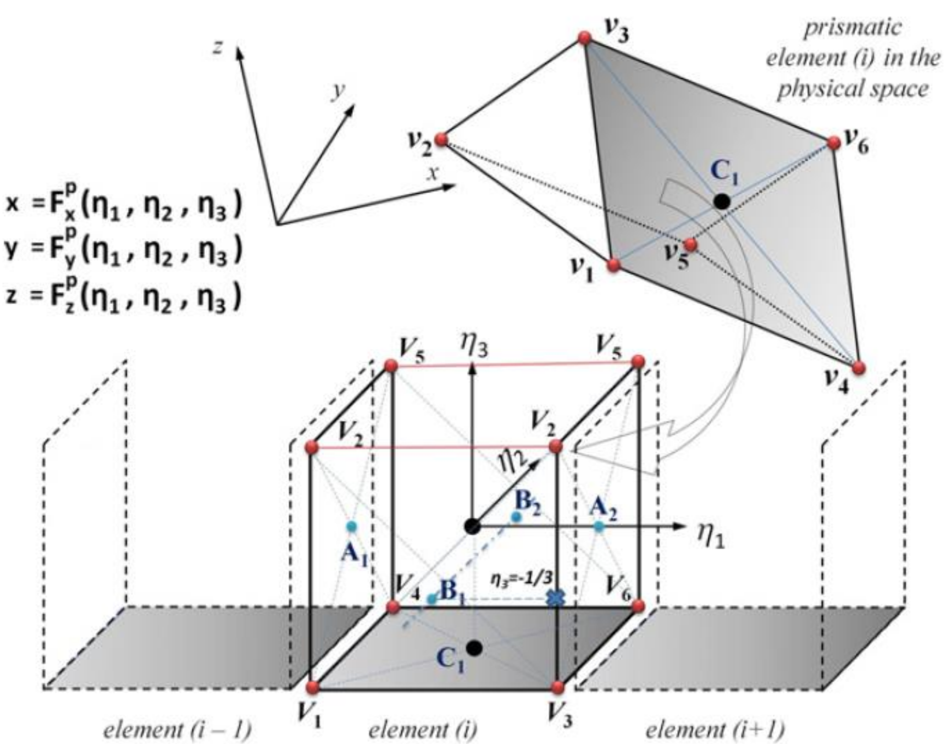

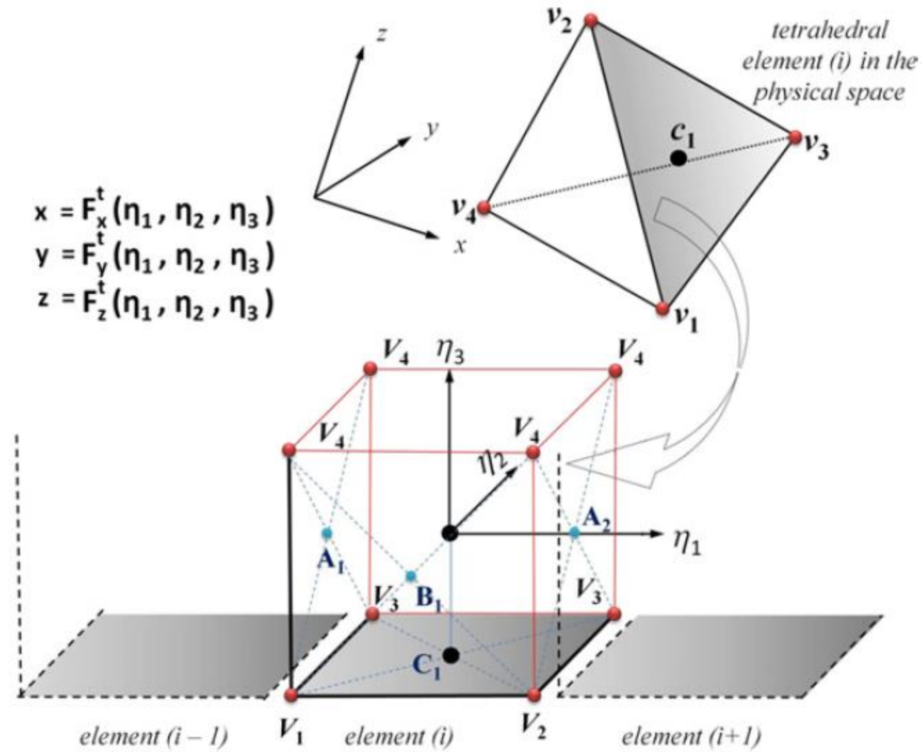

Why make all this trouble for the DG and not use FV with high resolution? Because of some DG features not found in FD or FV

- ✓ DG has a compact stencil and does nor require information from neighboring elements
- ✓ The compact stencil makes it particularly suitable for parallel processing with implicit or explicit time marching methods
- ✓ It is essentially a FE method therefore it well suited for *h*-, *p*-, or *h/p*-refinement, also in space-time FE/DG discretization
- ✓ It is well suited for problems with smooth solutions including complex features when high order expansions or p-type refinement is used
- ✓ It includes features from the FV methods that make possible capturing of strong discontinuities
- ✓ It does not require continuity of the solution at the element interface therefore application of adaptive mesh refinement (AMR) strategies with non-conforming elements (hanging nodes) becomes straight forward.
- ➢ It can naturally include high-order curved surface geometry (iso-geometric formulation)

A p-adaptive numerical solution of a linear problem

To satisfy the constraints for the divergence of the magnetic **B** and electric fields **E**, two new scalar potentials $\psi = \psi(x, y, z, t)$ and $\varphi = \varphi(x, y, z, t)$ are introduced

$$\frac{\partial \mathbf{B}}{\partial t} + \nabla \times \mathbf{E} + \boxed{\gamma \nabla \psi} = 0 \qquad \frac{\partial \mathbf{E}}{\partial t} - c^2 \nabla \times \mathbf{B} + \boxed{c^2 \chi \nabla \varphi} = c^2 \mu \mathbf{j}$$

$$\frac{\partial \psi}{\partial t} + \frac{\gamma}{\varepsilon \mu} \nabla \cdot \mathbf{B} = 0 \qquad \frac{\partial \varphi}{\partial t} + \chi \nabla \cdot \mathbf{E} = \chi \frac{\rho}{\varepsilon}$$

$\gamma, \chi \rightarrow c$ are sclar coefficients that can be considered as Lagrange multipliers

$$\int_E w_i \frac{\partial \mathbf{U}_h}{\partial t} dE + \underbrace{\int_E \nabla \cdot (w_i \mathbf{F}(\mathbf{U}_h))\, dE}_{} - \int_E \nabla w_i \cdot \mathbf{F}(\mathbf{U}_h)\, dE - \int_E w_i \mathbf{Q}_s dE = 0\ .$$

$$\mathbb{L}^E(\mathbf{U}_h) = \int_E w_i \frac{\partial \mathbf{U}_h}{\partial t} dE + \overbrace{\oint_{S_E} w_i \underbrace{\widehat{\mathbf{F}(\mathbf{U}_h) \cdot \mathbf{n}}}_{numerical\ flux} dS_E}^{Surface\ \ Integral}$$

$$- \int_E \nabla w_i \cdot \mathbf{F}(\mathbf{U}_h)\, dE - \int_E w_i \mathbf{Q}_s dE = 0.$$

p-refined numerical solutions

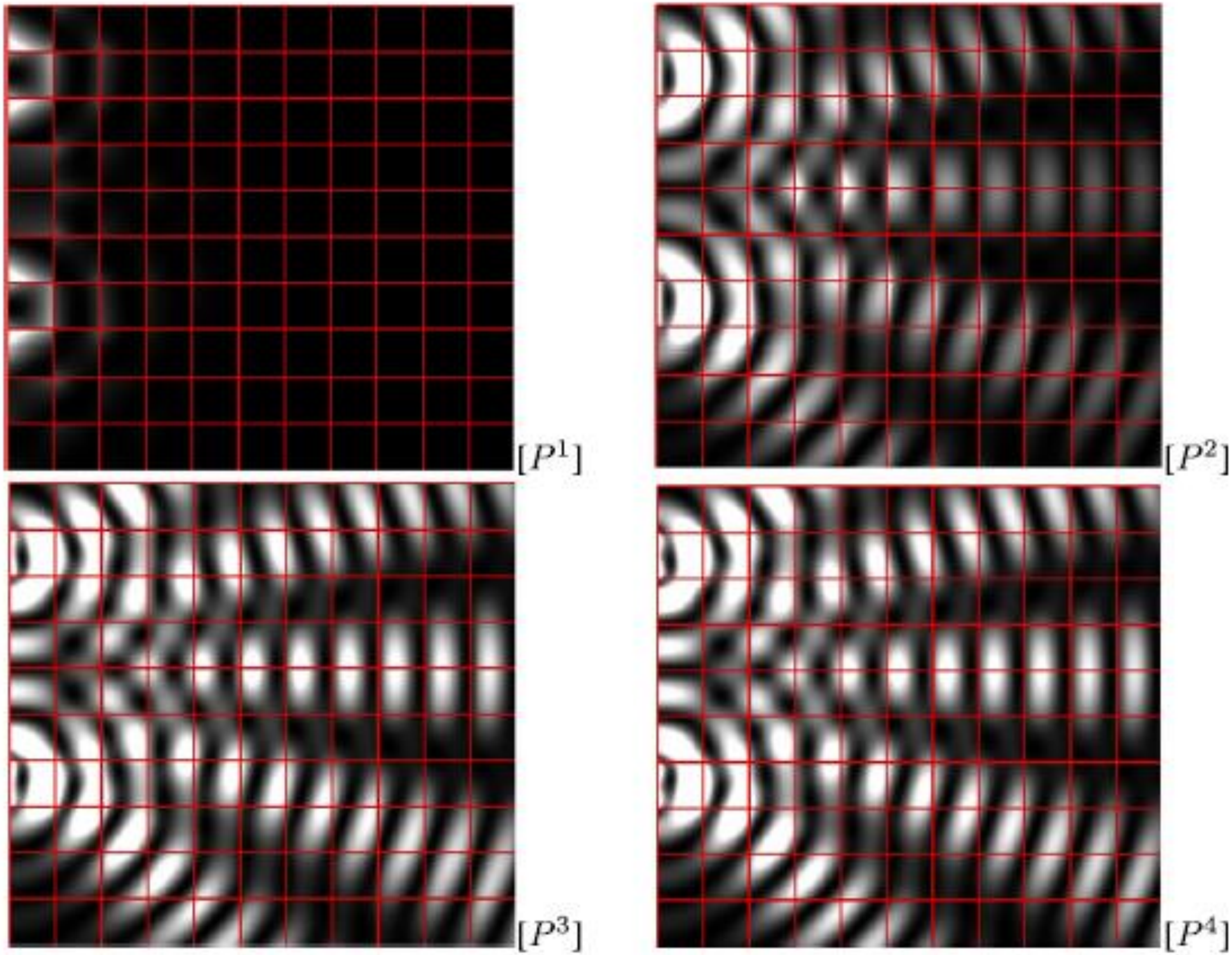

p-adapted numerical solution

$$dg_{E_i} = \left(\prod g\right)_{E_i} = \sum_{P_i} \left(\prod^{P_i} g\right)_{E_i} \phi_i^p = \sum_{P_i} \frac{(\phi_i^p, g)_{E_i}}{(\phi_i^p, \phi_i^p)_{E_i}} \phi_i^p .$$

Project the solution to the neighboring element

$$||\epsilon_k||_{L_2} = ||\mathbf{u}_{ref} - \mathbf{U}_h^k||_{L_2} = \left(\sum_{E_i \in E} ||\mathbf{u}_{ref} - \mathbf{U}_{ref}||_{E_i}\right)^{1/2}$$

$$= \left(\sum_{E_i \in E} ||\mathbf{u}_{ref} - \prod_h^k \mathbf{u}_{ref}||_{E_i}\right)^{1/2} \leqslant \left(\sum_{E_i \in E} ||\epsilon_{k_i}||_{E_i}^2\right)^{1/2},$$

Compute the error and ensure that it is bellow a prescribed tolerance

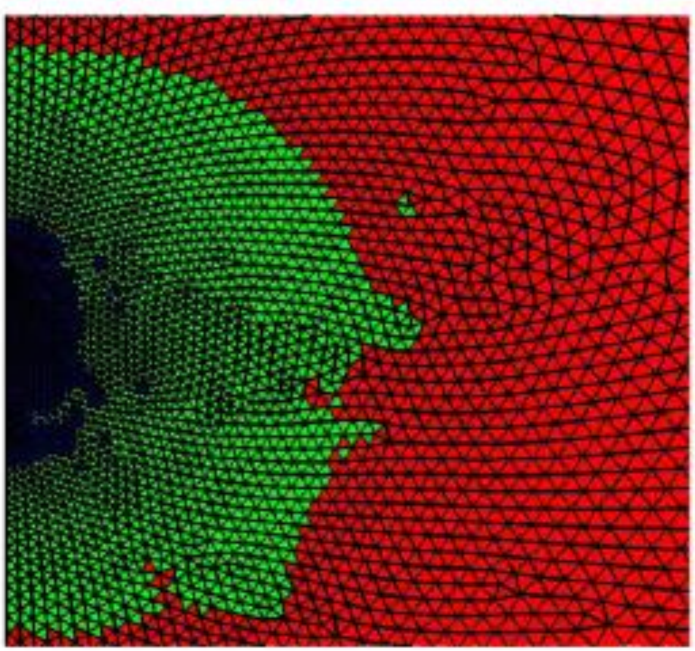

Application of p-adaptivity, P2 (blue), P3 (green), and P4 (red) for a prismatic nonuniform mesh.

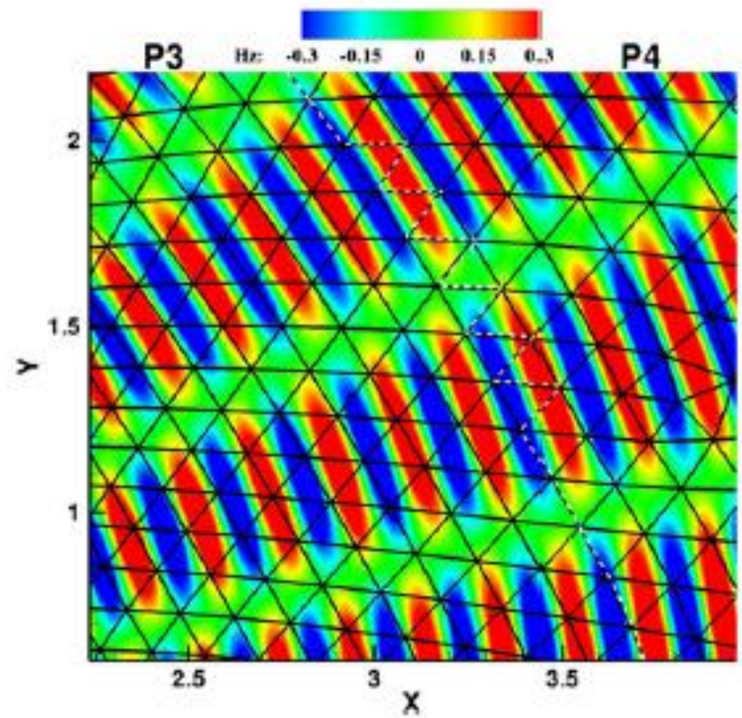

Visualization of the the computed waves. The dashed line marks the border for the transition from P3 to P4

Computed p-adaptive numerical solution for aircraft radar cross-section

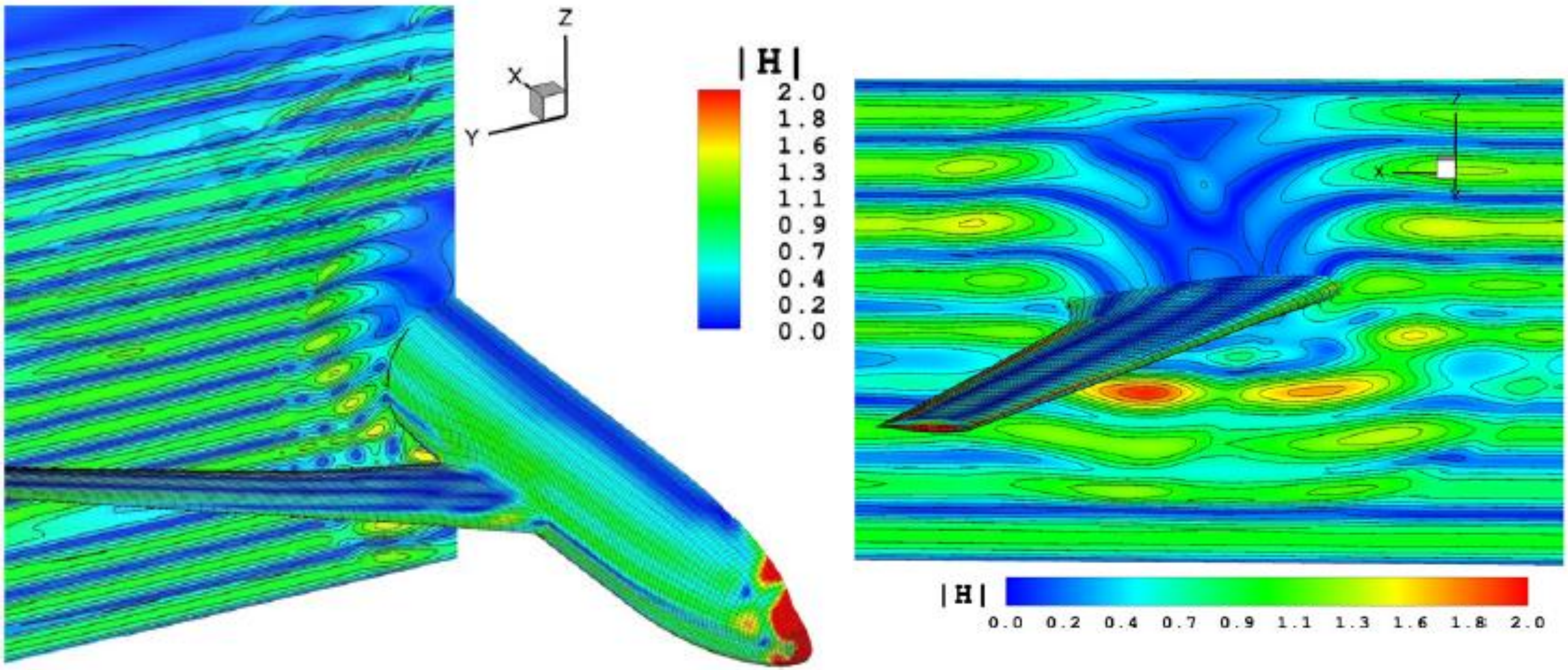

ERAU

TVB and TVD limiting for discontinuity capturing

- To eliminate oscillations at strong discontinuities of both the flow field and the electromagnetic field variable the following TVB limiter is used

$$\bar{m}(a_1, a_2, a_3) = \begin{cases} a_1 & \text{if } |a_1| \le \wp L^2 \\ m(a_1, a_2, a_3) & \text{otherwise} \end{cases}$$

the parameter $\wp$ is an estimation of second order derivative of variable u and it is estimated by the Laplacian $\wp(u) \approx \nabla^2 u$ in the transformed space

- The TVB limiter is applied to the characteristic variables of the flow field
- TVB Limiting is performed in the transformed canonical space of cubic elements to the characteristic variables and the limited variables are transferred back to the physical domain using collapsed coordinates
- Limiting is applied for all variable at the end of each RK stage
- TVD limiting can be applied in the physical space it is more diffusive than the TVB limiter and the computational cost is not very low

TVB and hierarchical limiters

Hierarchical Limiter

$$u_h^h = \sum_{i=0}^{26} c_i^h b_i^h$$

$$\begin{aligned}\widetilde{c_i^h} = m\big(c_i^h,\,&(\alpha_1/L)(c^h_{l,(i+1,j,k)} - c^h_{l,(i,j,k)}), (\alpha_1/L)(c^h_{l,(i,j,k)} - c^h_{l,(i-1,j,k)}),\\ &(\alpha_2/L)(c^h_{m,(i,j+1,k)} - c^h_{m,(i,j,k)}), (\alpha_2/L)(c^h_{m,(i,j,k)} - c^h_{m,(i,j-1,k)}),\\ &(\alpha_3/L)(c^h_{n,(i,j,k+1)} - c^h_{n,(i,j,k)}), (\alpha_3/L)(c^h_{n,(i,j,k)} - c^h_{n,(i-1,j,k-1)})\big)\end{aligned}$$

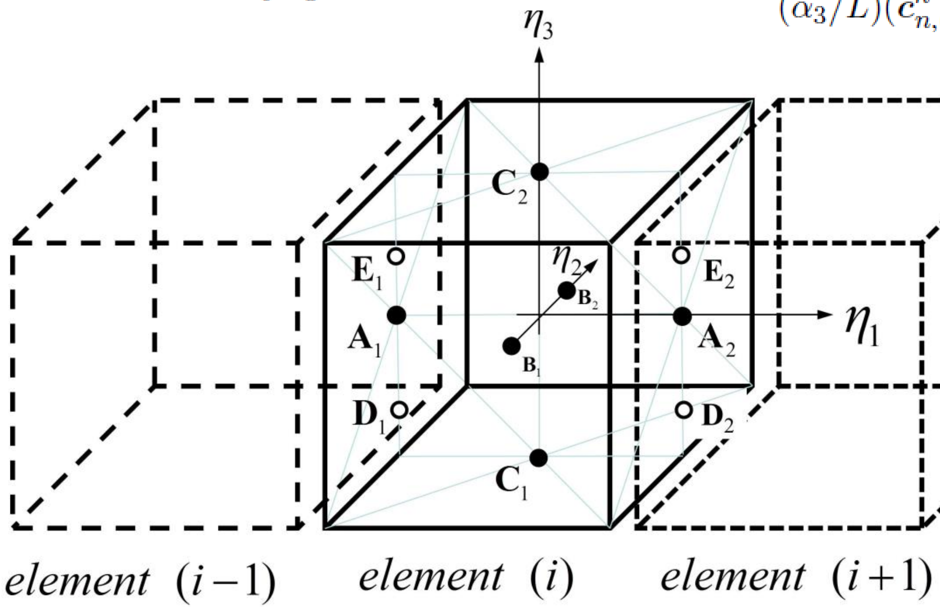

P1 Limiter

$$\overline{m}(a_1, a_2, \ldots, a_n) = \begin{cases} a_1 & \text{if } |a_1| \le M L^2_{x,y,z} + b, \\ m(a_1, a_2, \ldots, a_n) & \text{otherwise.} \end{cases}$$

$$\begin{aligned} u_h^h = c_0^h + c_1^h\eta_1 &+ c_2^h\eta_2 + c_3^h\eta_3 \\ &+ c_4^h\eta_1\eta_2 + c_5^h\eta_1\eta_3 + c_6^h\eta_2\eta_3 \\ &+ c_7^h\eta_1\eta_2\eta_3 \end{aligned}$$

$$U_{A_1} = u^h(-1,0,0) - c_0^h = -c_1^h,$$

$$U_{A_2} = u^h(1,0,0) - c_0^h = c_1^h,$$

$$\widetilde{U}_{A_1} = -m(-U_{A_1}, c^h_{0,(i+1,j,k)} - c^h_{0,(i,j,k)}, c^h_{0,(i,j.k)} - c^h_{0,(i-1,j,k)}),$$

$$\widetilde{U}_{A_2} = m(U_{A_2}, c^h_{0,(i+1,j,k)} - c^h_{0,(i,j,k)}, c^h_{0,(i,j,k)} - c^h_{0,(i-1,j,k)}),$$

$$\widetilde{c}_1^h = \frac{\widetilde{U}_{A_2} - \widetilde{U}_{A_1}}{2}.$$

Adaptive mesh refinement with P1+TVB limiter for enhanced resolution of discontinuities and complex flow features

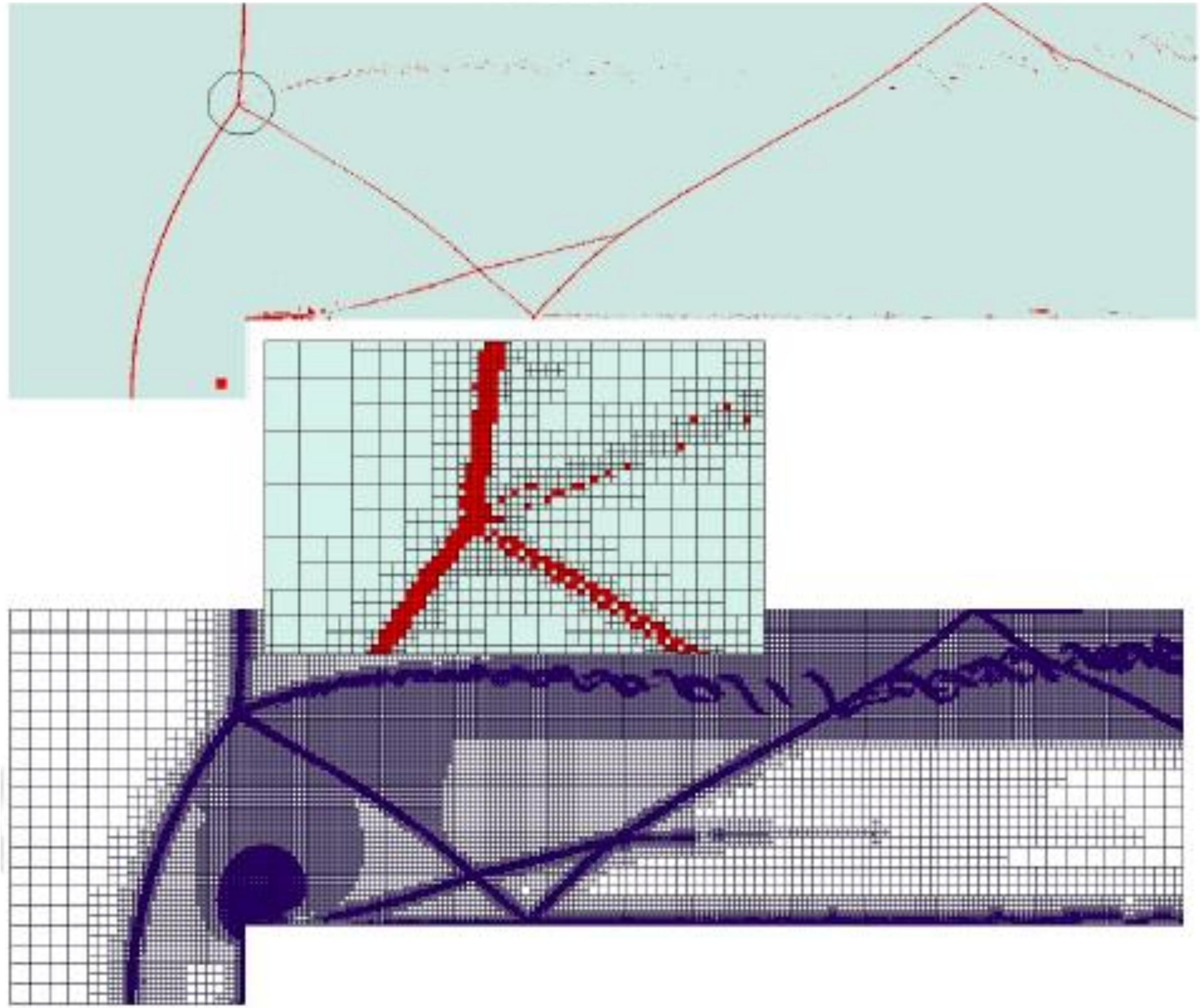

Adaptive mesh refinement and parallel efficiency

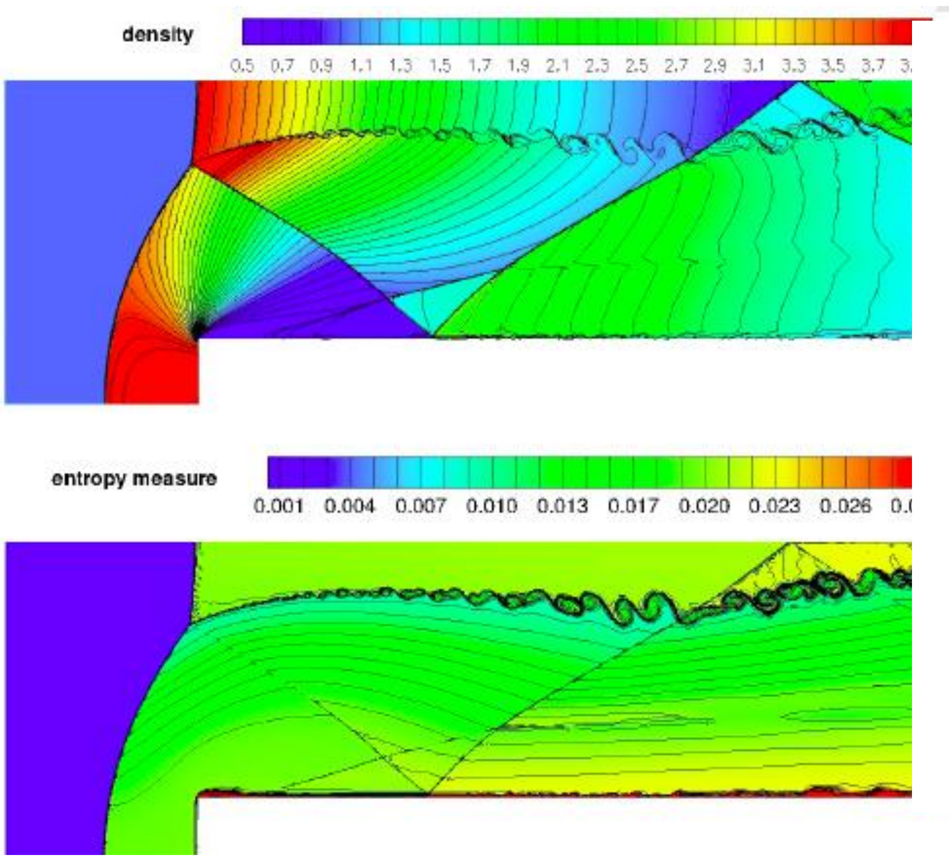

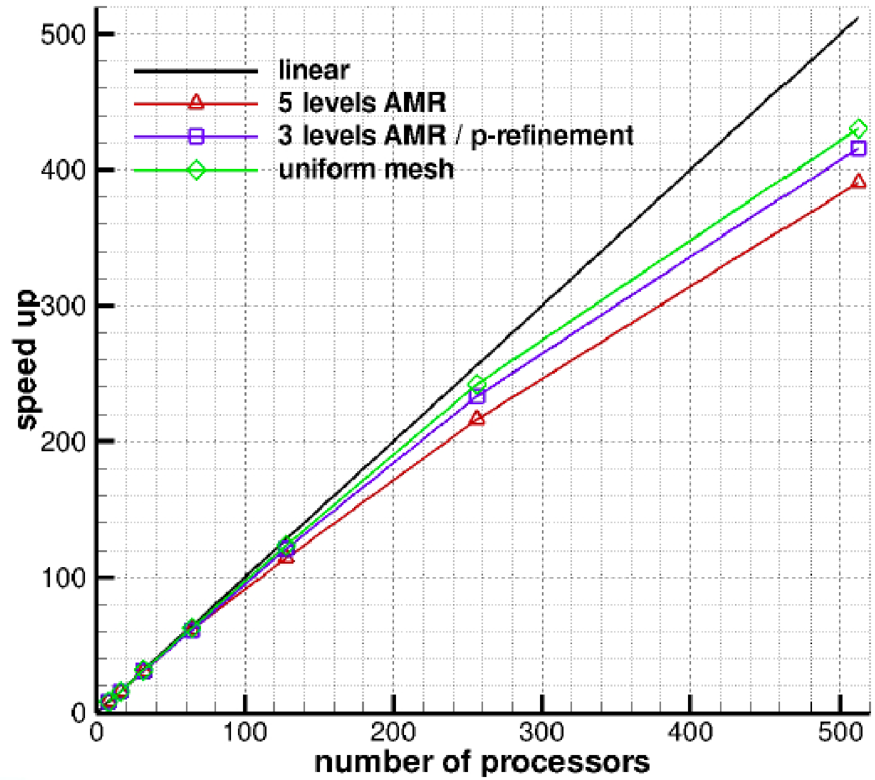

Adaptive mesh refinement on discontinuities and smooth complex flow features

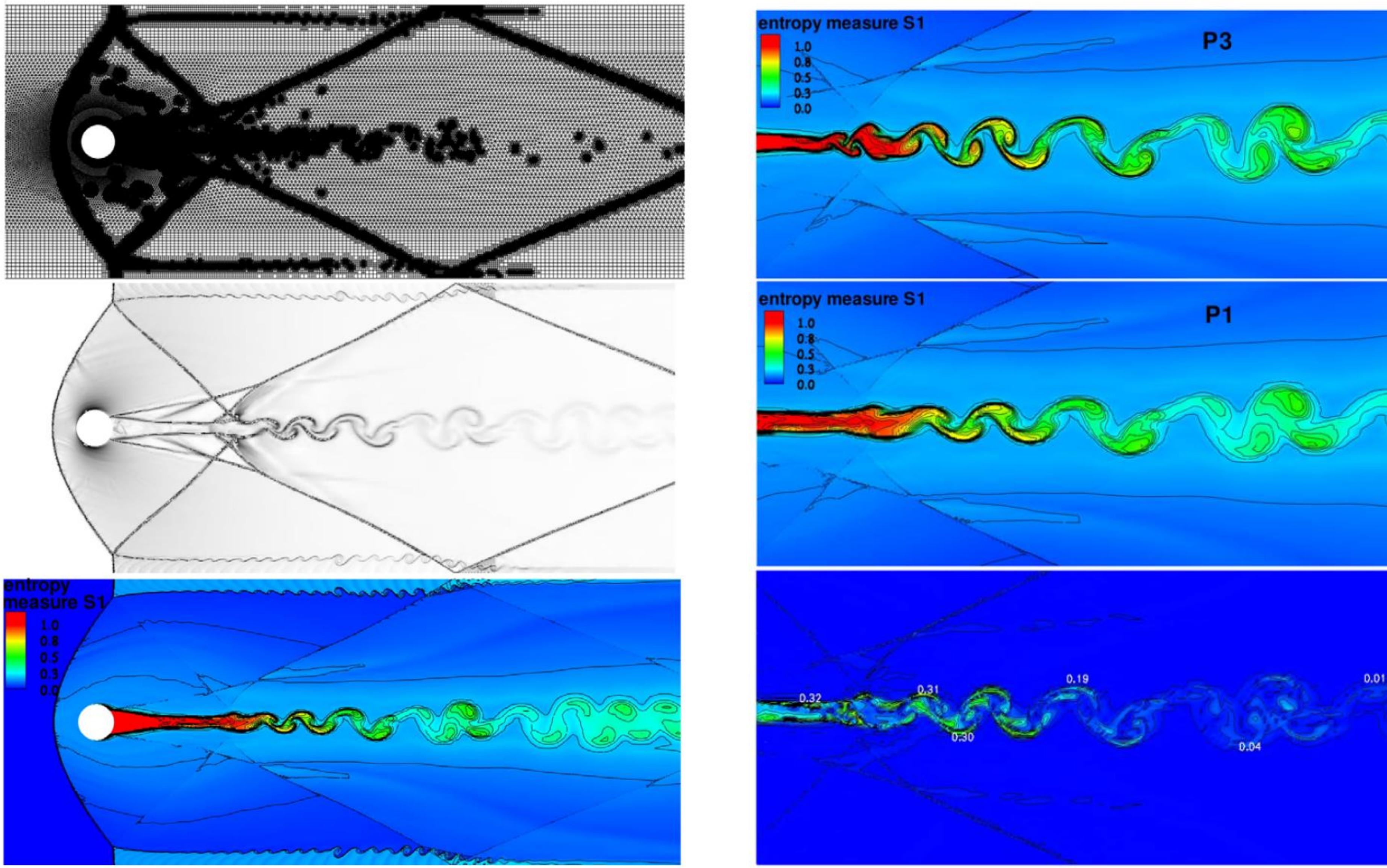

The dissipative filter for P1 or higher-order expansions

Let $\boldsymbol{LF_x}$ be the dissipative flux of the filter operator along the x direction with similar definitions for $\boldsymbol{LFy}$ and $\boldsymbol{LFz}$ along the other directions

$$\mathbf{LF}_x(F^*) = \frac{1}{\Delta x}\left[F^*_{i+1/2} - F^*_{i-1/2}\right]$$

$$U^{n+1} = \hat{U}^{n+1} + \left(\Delta t\right)\left[\mathbf{LF}_x(F^*) + \mathbf{LF}_y(G^*) + \mathbf{LF}_z(H^*)\right]$$
$$= \hat{U}^{n+1} + \left(\Delta t\right)\mathbf{LF}$$

and in the finite element context

$$\int_{\Omega_{\mathrm{m}}} wU^{n+1} d\Omega_{\mathrm{m}} = \int_{\Omega_{\mathrm{m}}} wU^{n+1} d\Omega_{\mathrm{m}} + \left(\Delta t\right)\int_{\Omega_{\mathrm{m}}} w\,\mathbf{LF}\,d\Omega_{\mathrm{m}}$$

The filter dissipative fluxes

$$F^*_{i+1/2} = \frac{1}{2} R_{i+1/2} \, \Phi^*_{i+1/2}$$

$R_{i+1/2}$ are the right eigenvectors evaluated at Roe's averae state and the elements φ^* of the matrix $\Phi^*_{i+1/2}$ are given by

$$\varphi^*_{i+1/2} = \kappa \; \theta_{i+1/2} \; \varphi_{i+1/2}$$

the function $\kappa \; \theta_{i+1/2}$ plays the role of discontinuity detector

where $0.03 < \kappa < 2$

or it is evaluated based on the smothness of computed solution

and $\theta_{i+1/2}$ is evaluated as suggested by Yee

$$\theta_{i+1/2} = \max\left(\hat{\theta}_{i-m+1}, \ldots, \hat{\theta}_{i+m}\right) \quad \hat{\theta}_i = \left| \frac{\left|r_{i+1/2}\right| - \left|r_{i-1/2}\right|}{\left|r_{i+1/2}\right| + \left|r_{i-1/2}\right|} \right|^p$$

where $r_{i+1/2}$ are the elements of $R^{-1}_{i+1/2} \Delta U$

Application of the filter in 1D for P1, P2, and P3 expansions using information from neighboring elements

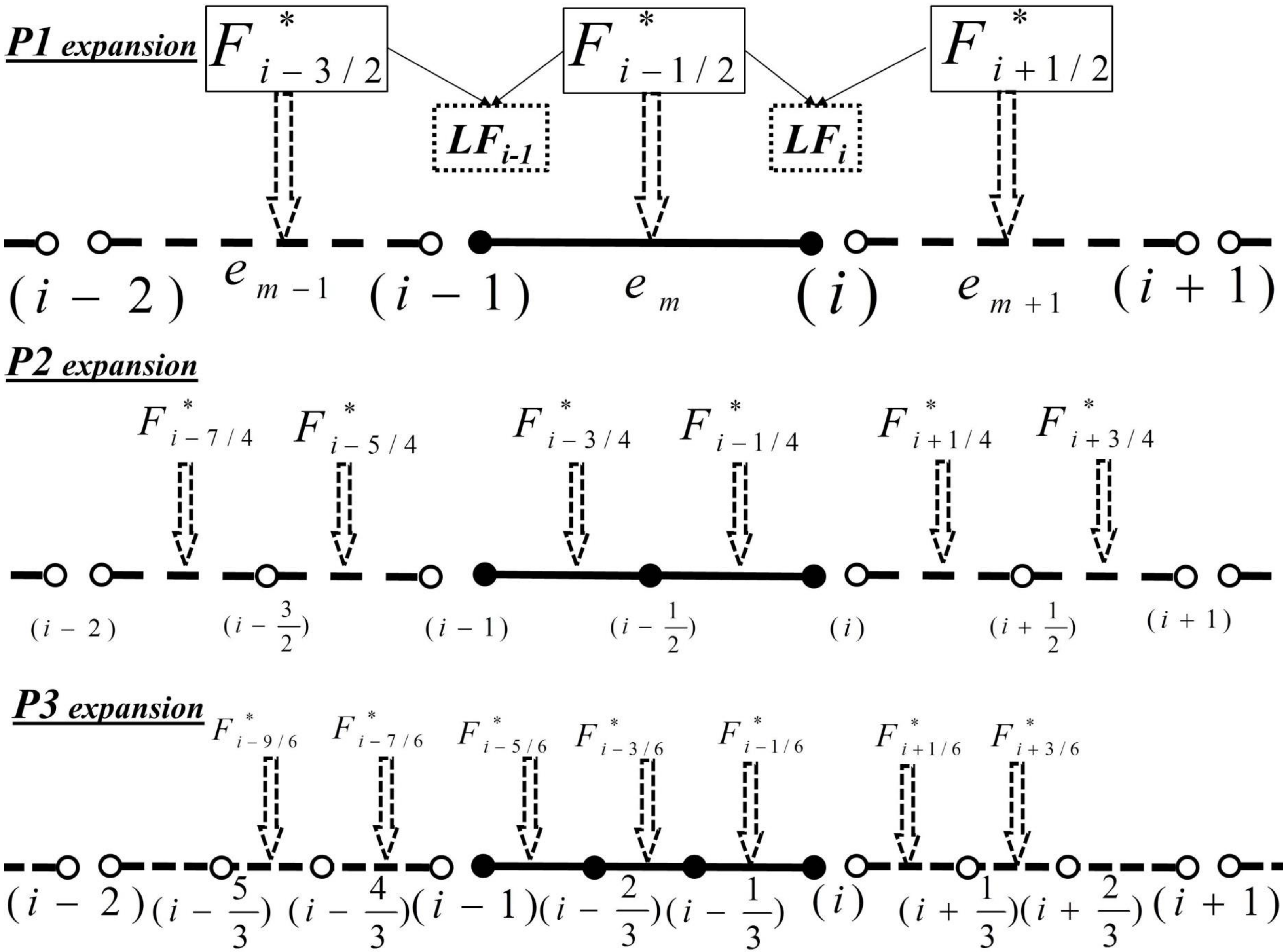

Application of the filter for quadrilateral elements

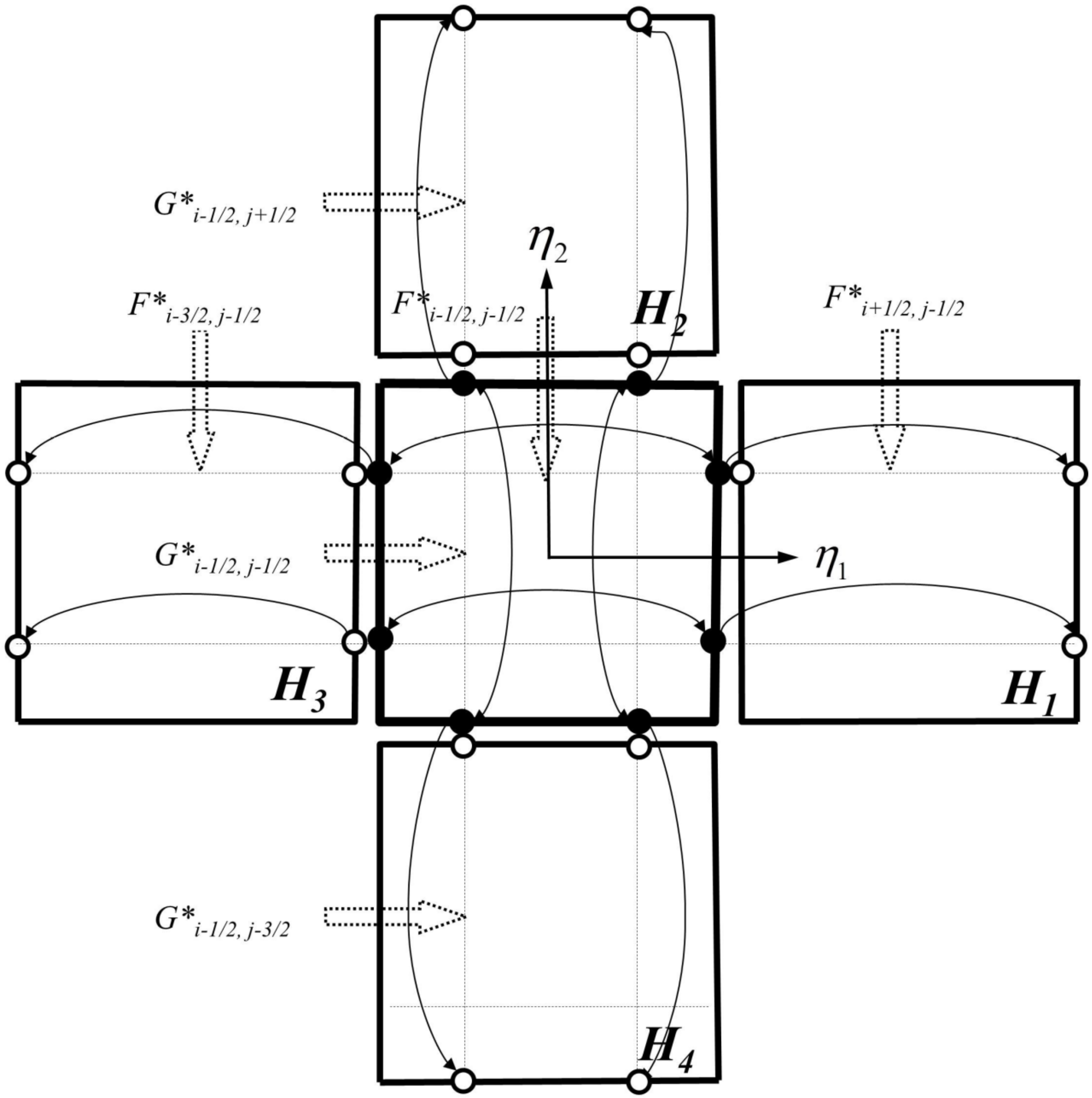

Application of the filter for triangular elements

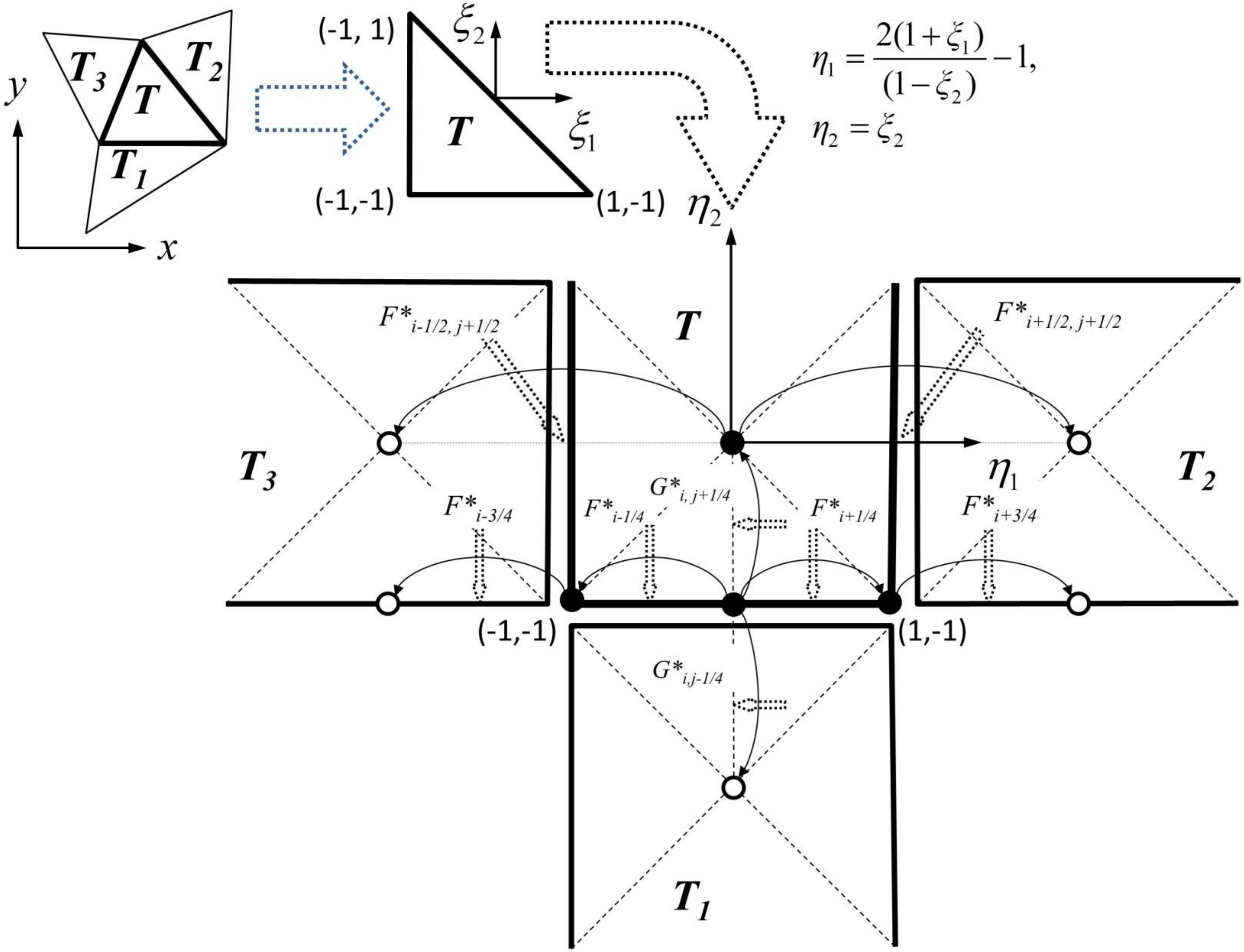

$$\eta_1 = \frac{2(1+\xi_1)}{(1-\xi_2)} - 1,$$
$$\eta_2 = \xi_2$$

Application of the filter in 1D for P1, P2, and P3 expansions with oversampling and information only from the element

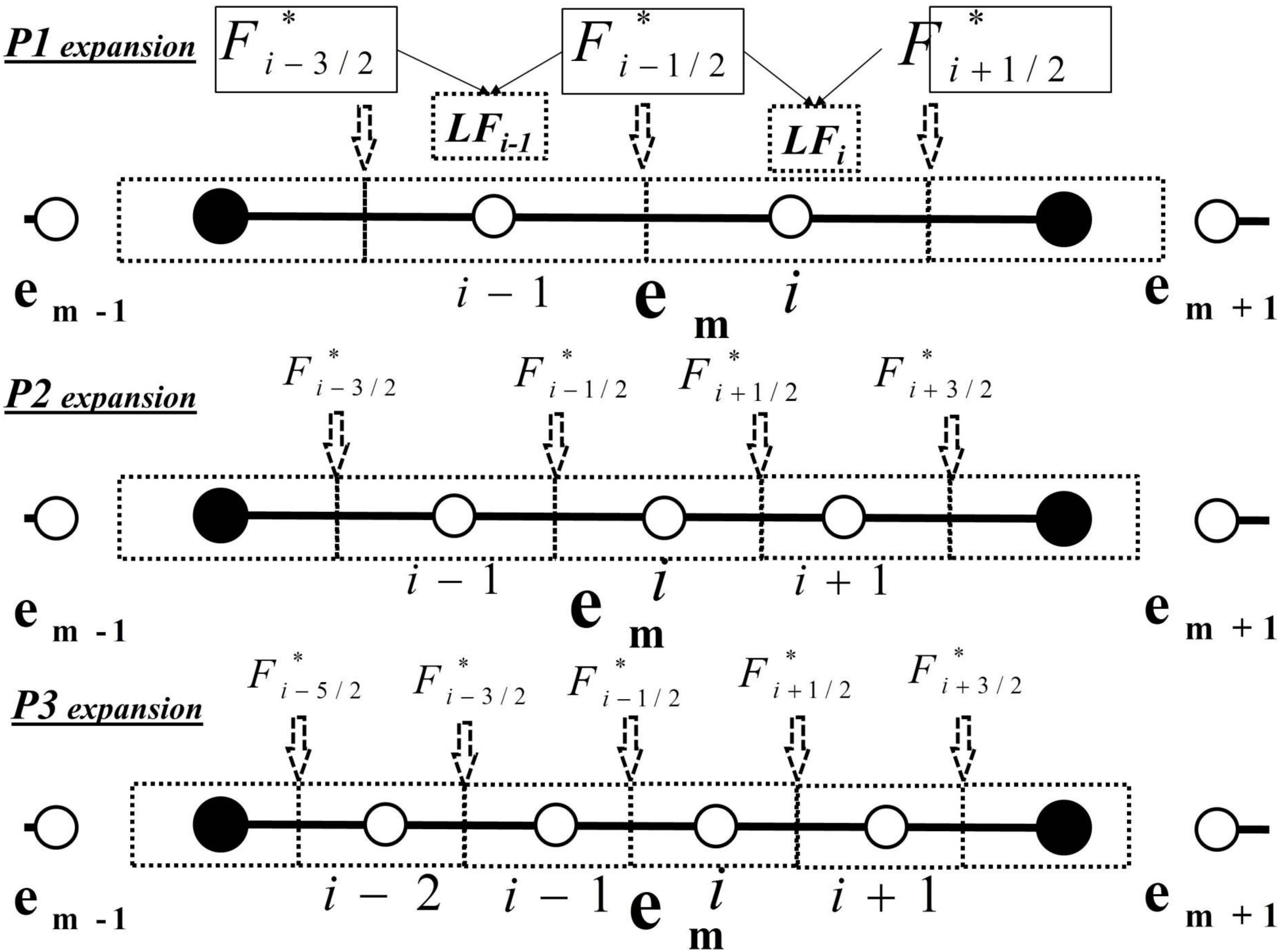

Higher order reconstruction would be required to avoid oversampling

- Use the hybridazable DG and reconstruct the numerical solution to one order higher (p to p+1) for the filter construction

- Use the recovered function (van Leer) to construct the filter operator

- Use higher order reconstruction within the element by projecting the recovered function to construct the filter operator

Oversampling and least square projection is chosen

Application of the filter for a smooth problem computed with centered flux

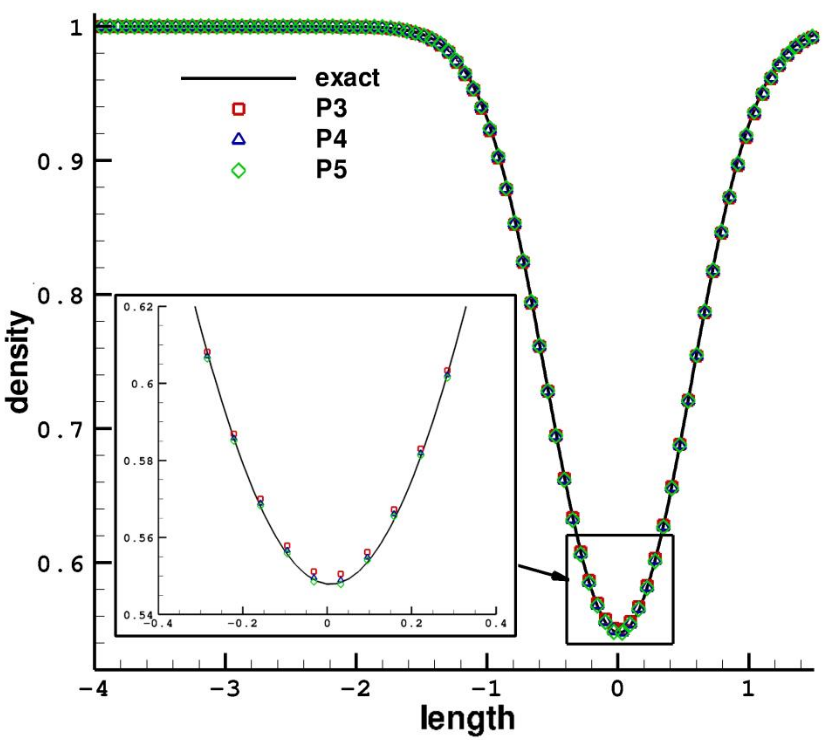

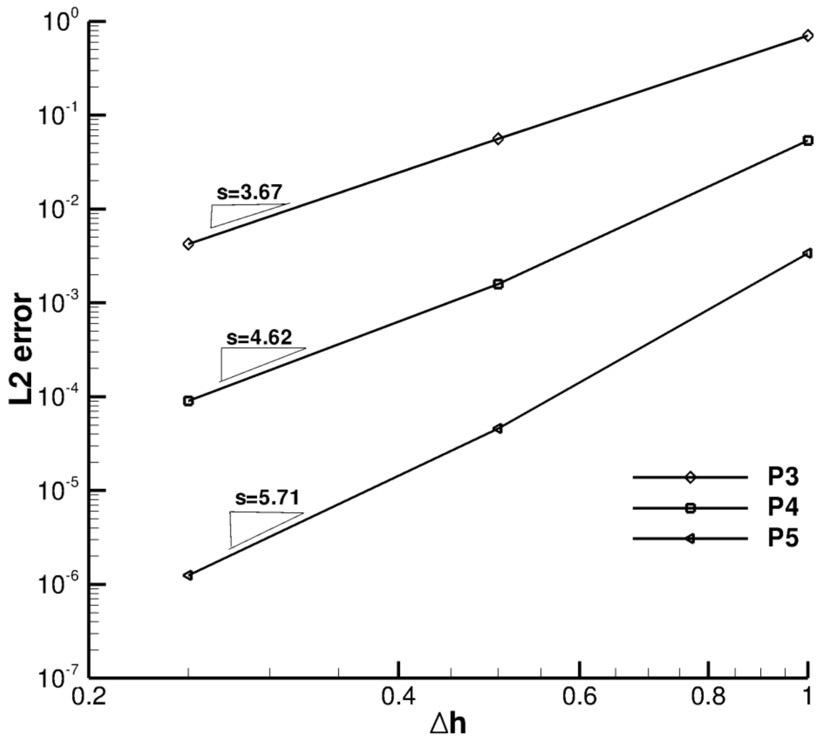

Application of the filter for the Sod's shock tube problem
Filter constructed using neighboring elements

200 elements h = 0.01

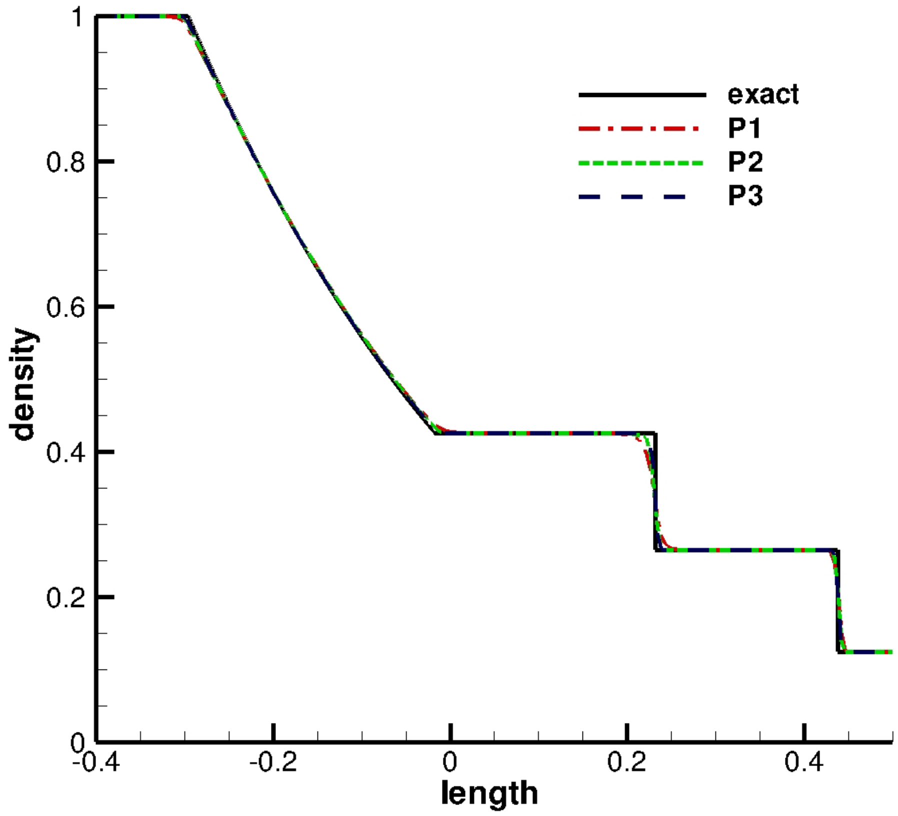

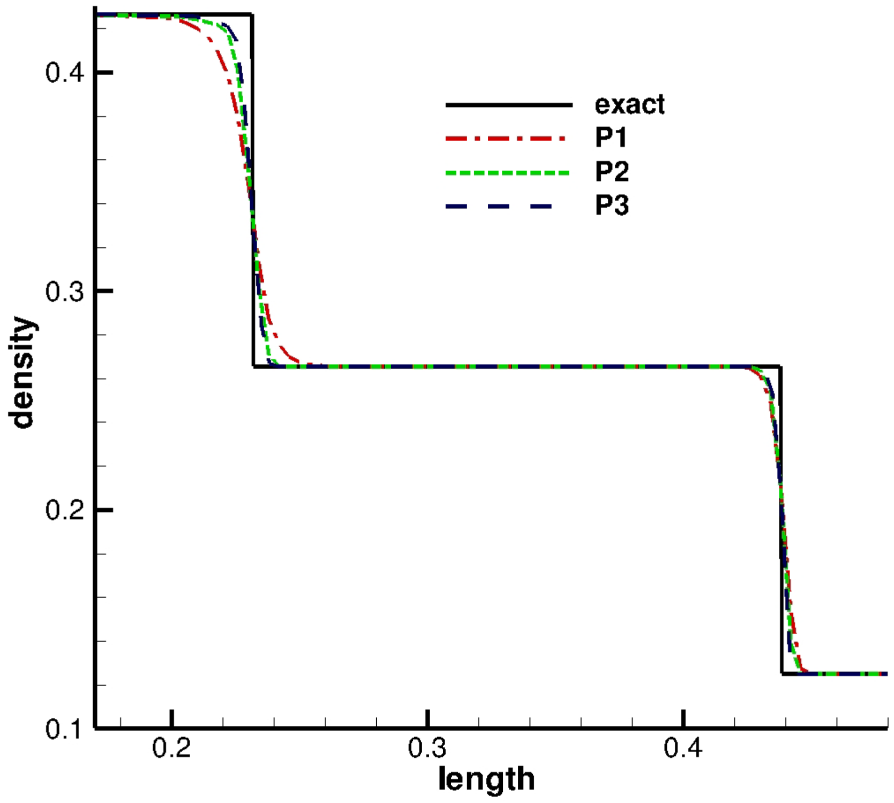

Filter operator projection with P4, h = 1/5 and in the cell discontinuity capturing

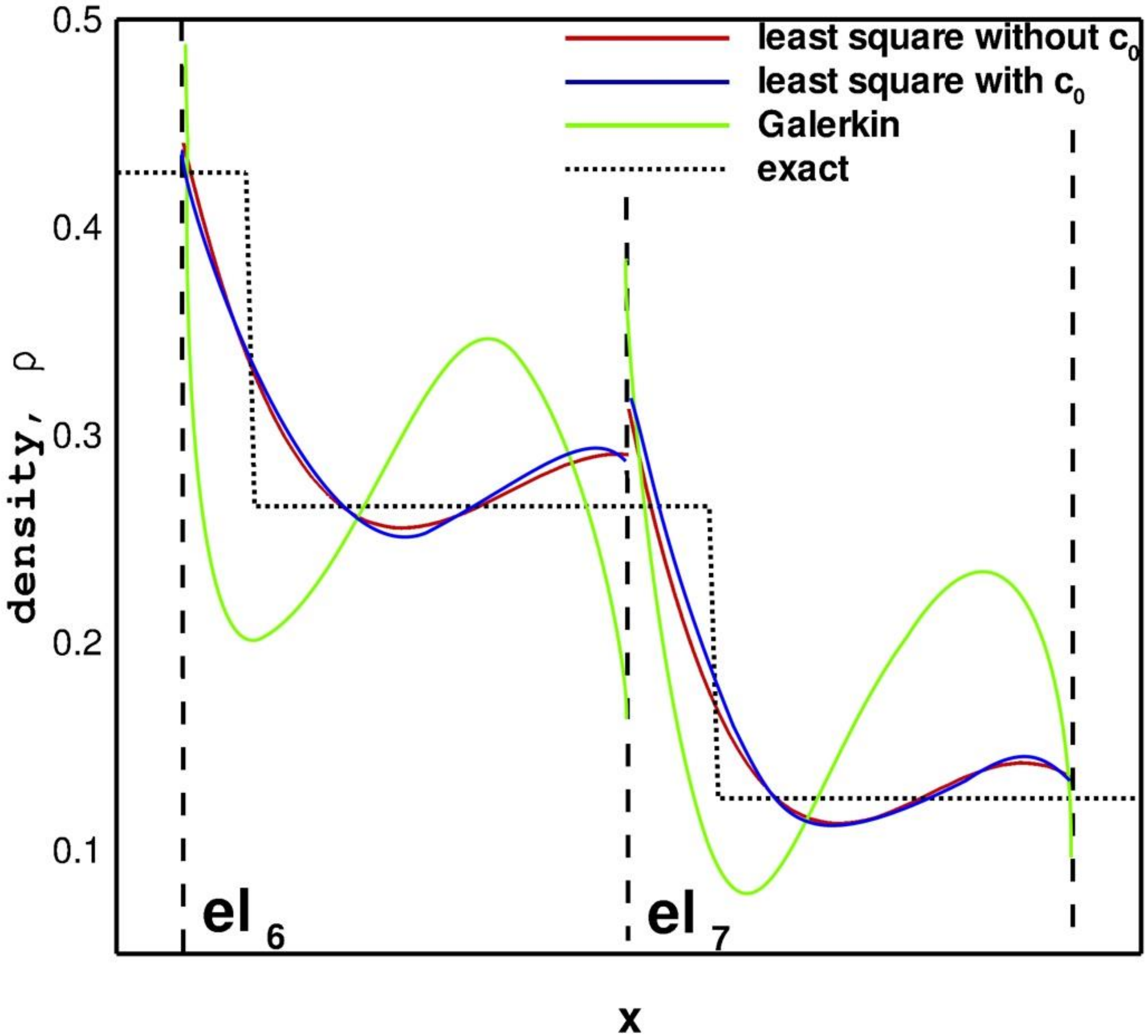

- The Galerkin projection appears more oscillatory and affects the solution average (c_0)
- Least square projection is less oscillatory and it does not require to modify the computed solution average in the spirit of TVB limiters

Application of the filter for the Sod's shock tube problem sub-cell discontinuity capturing filter in the element

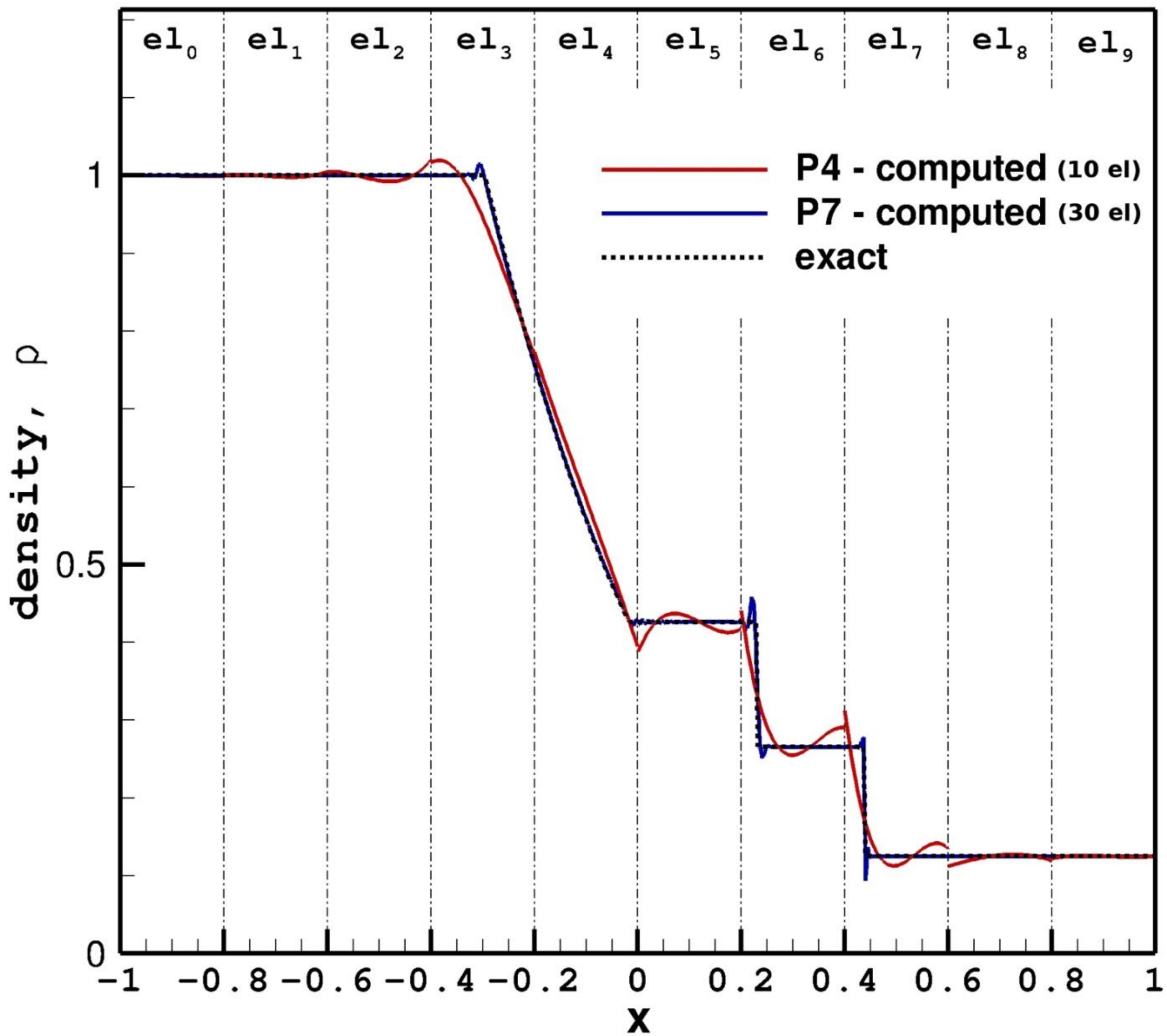

P4 h = 1/5

P7 h = 1/15

Galerkin and least square projection of the filter

Sod problem P4 numerical solution

very coarse mesh with 10 elements h = 0.2

Oversampled solution within the cell

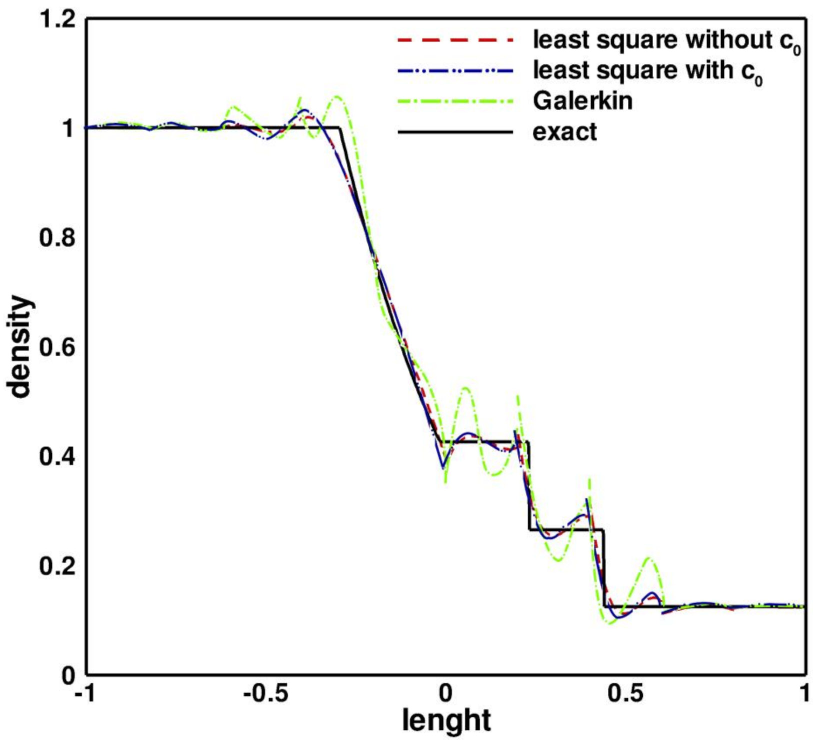

Filter constructed from higher order reconstructed Hybridizable DG solution

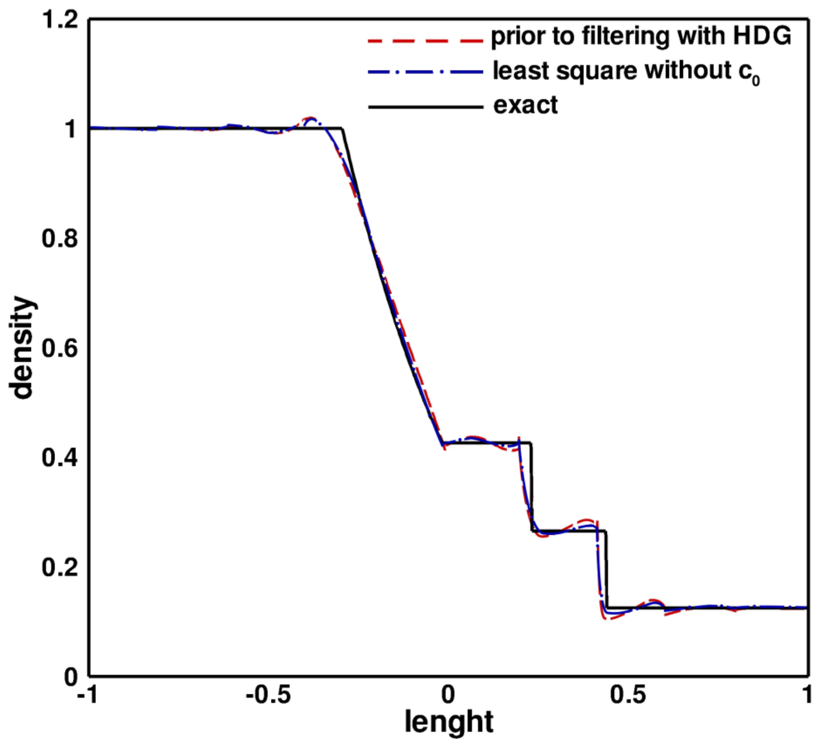

Application of the filter for the Sod's shock tube problem
Filter constructed <u>within the element</u>

20 elements h = 0.1

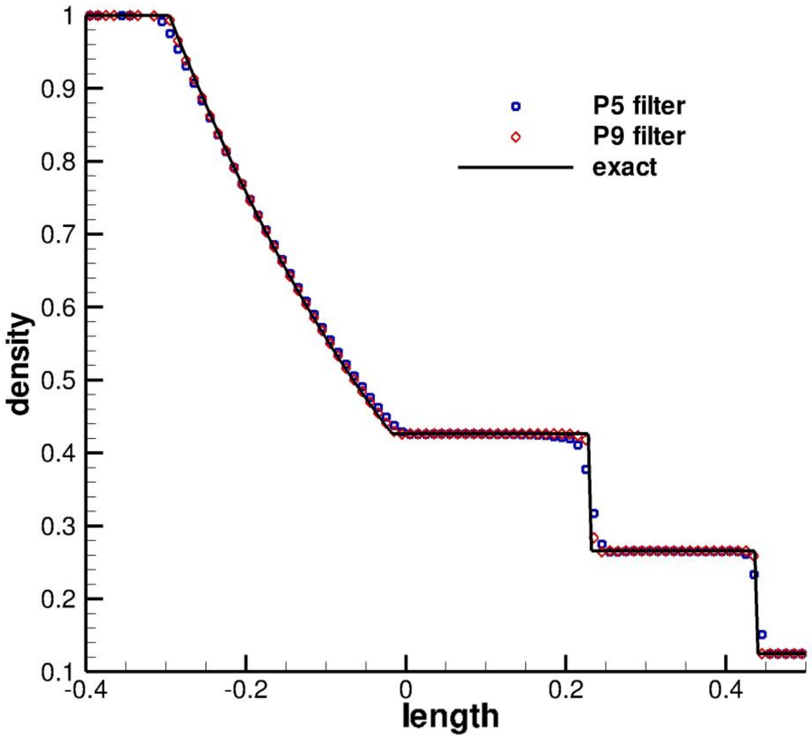

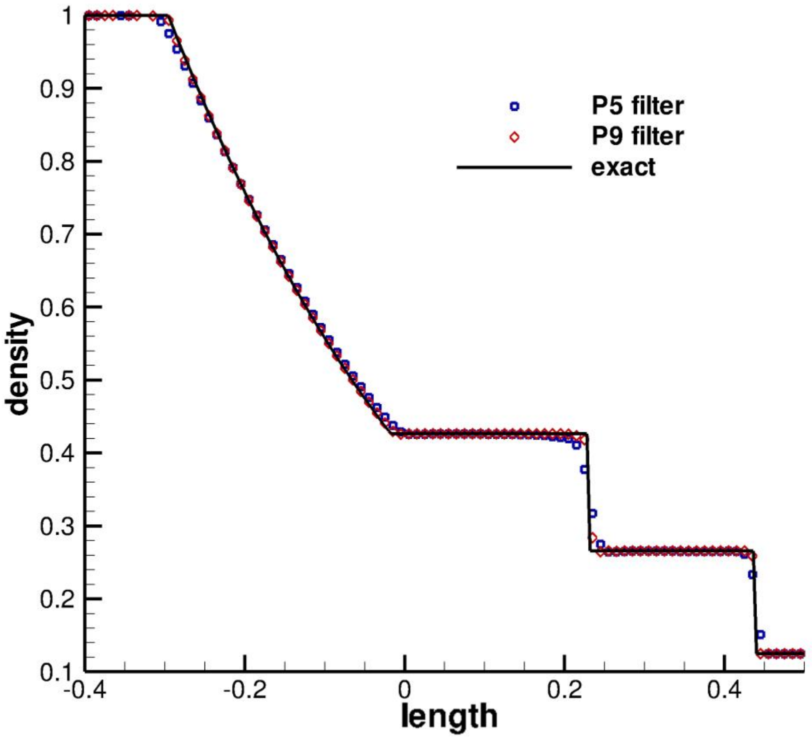

Convergence rate for the Sod's shock tube problem filter operator from the element

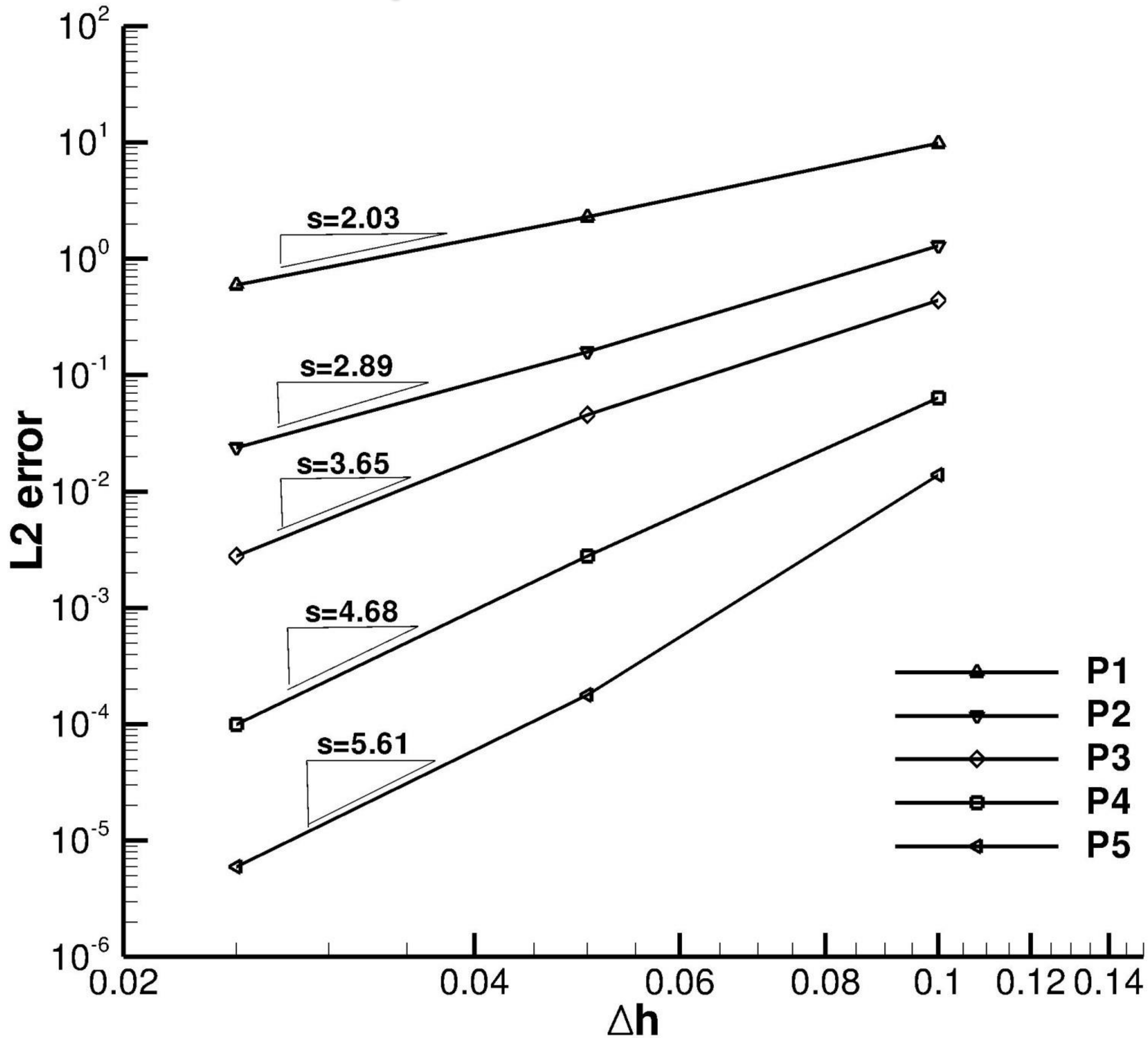

Large pressure ratio shock tube problem
Filter constructed using neighboring elements

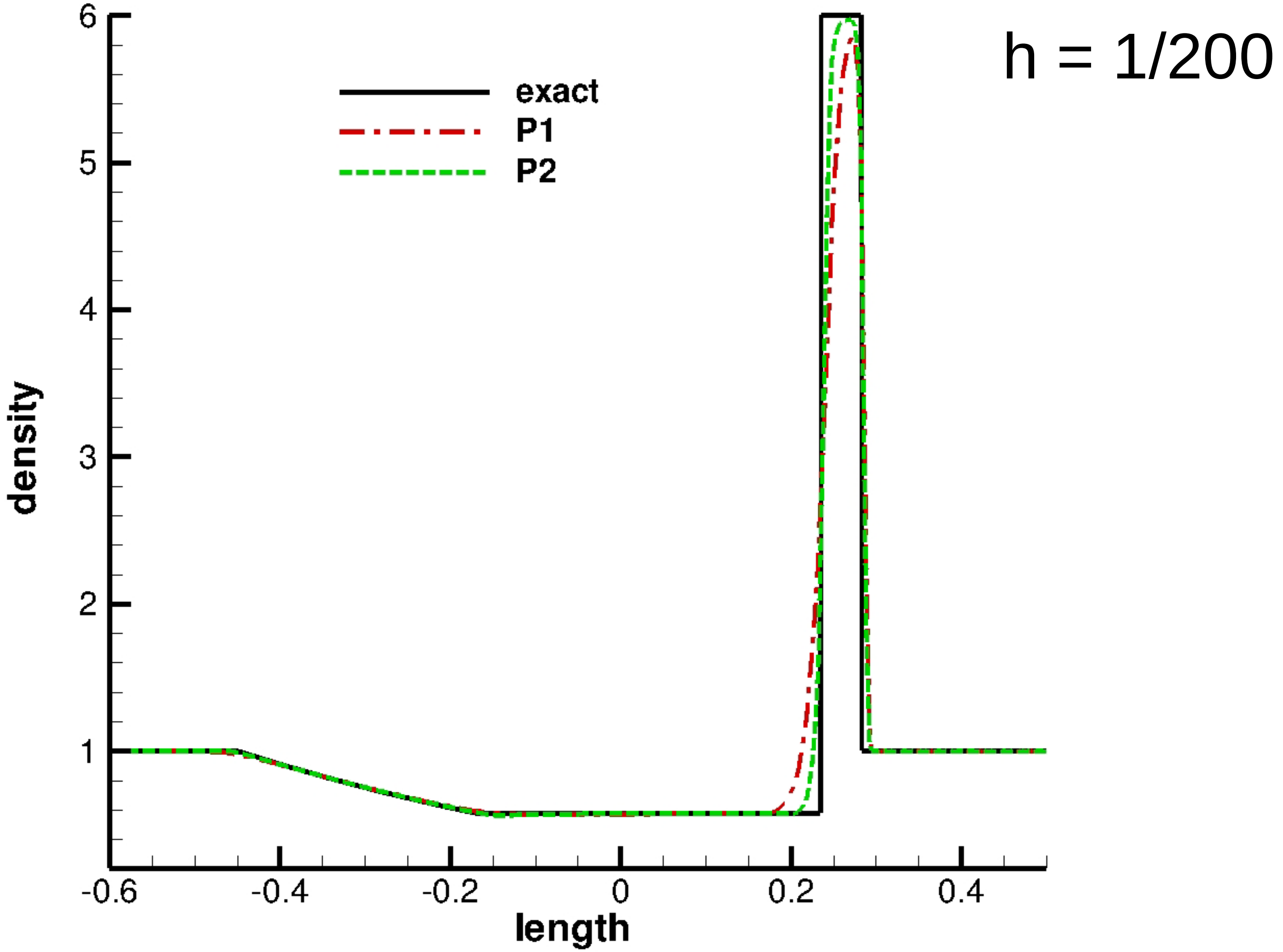

Large pressure ratio shock tube problem
Filter constructed within the element

Filtered h = 1 / 40, TVB hierarchical h = 1/400

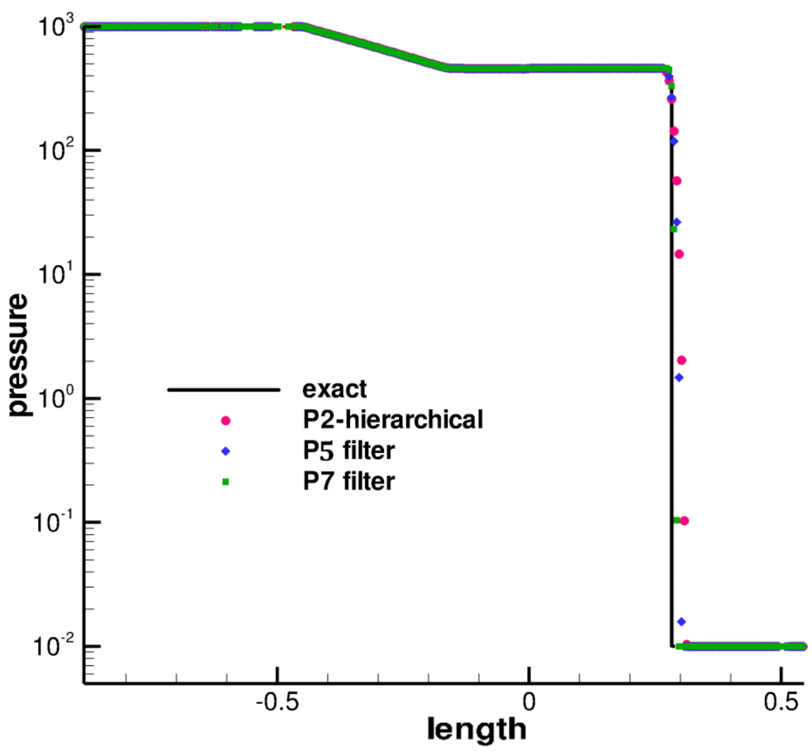

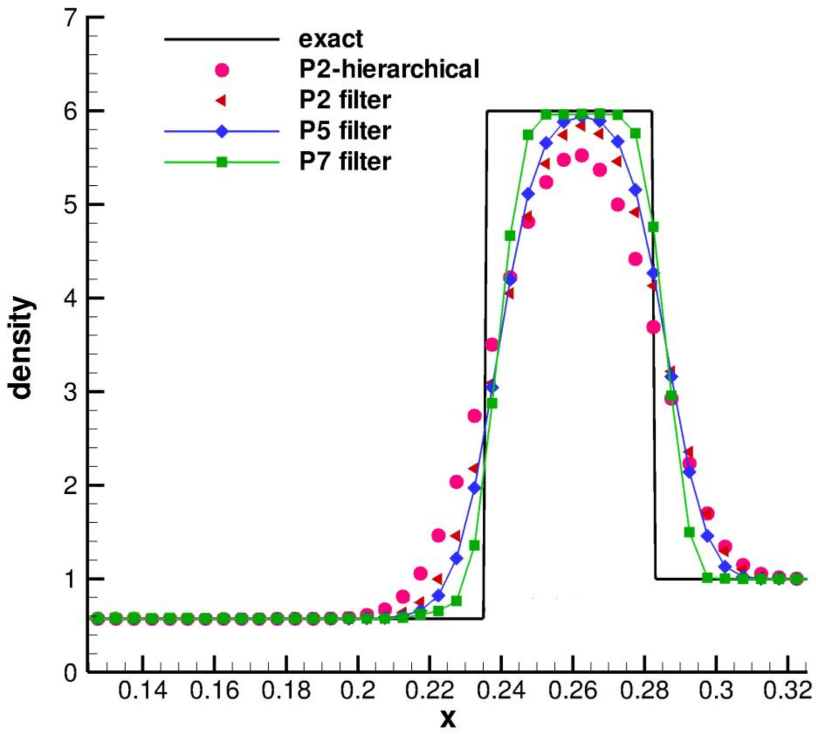

Shu and Osher density perturbation shock interaction using information from neighboring elements

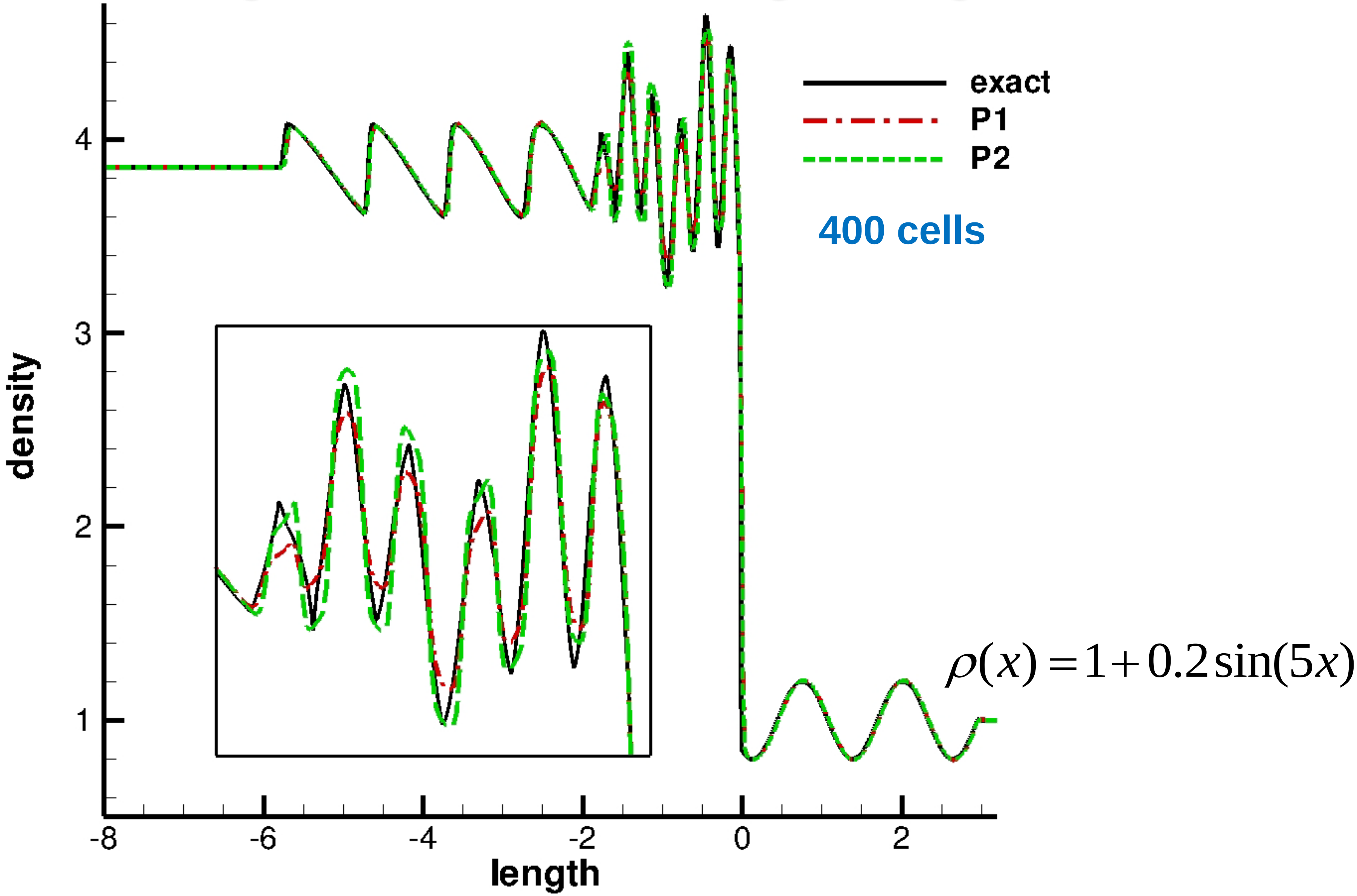

Shu and Osher density perturbation shock interaction using information from the element

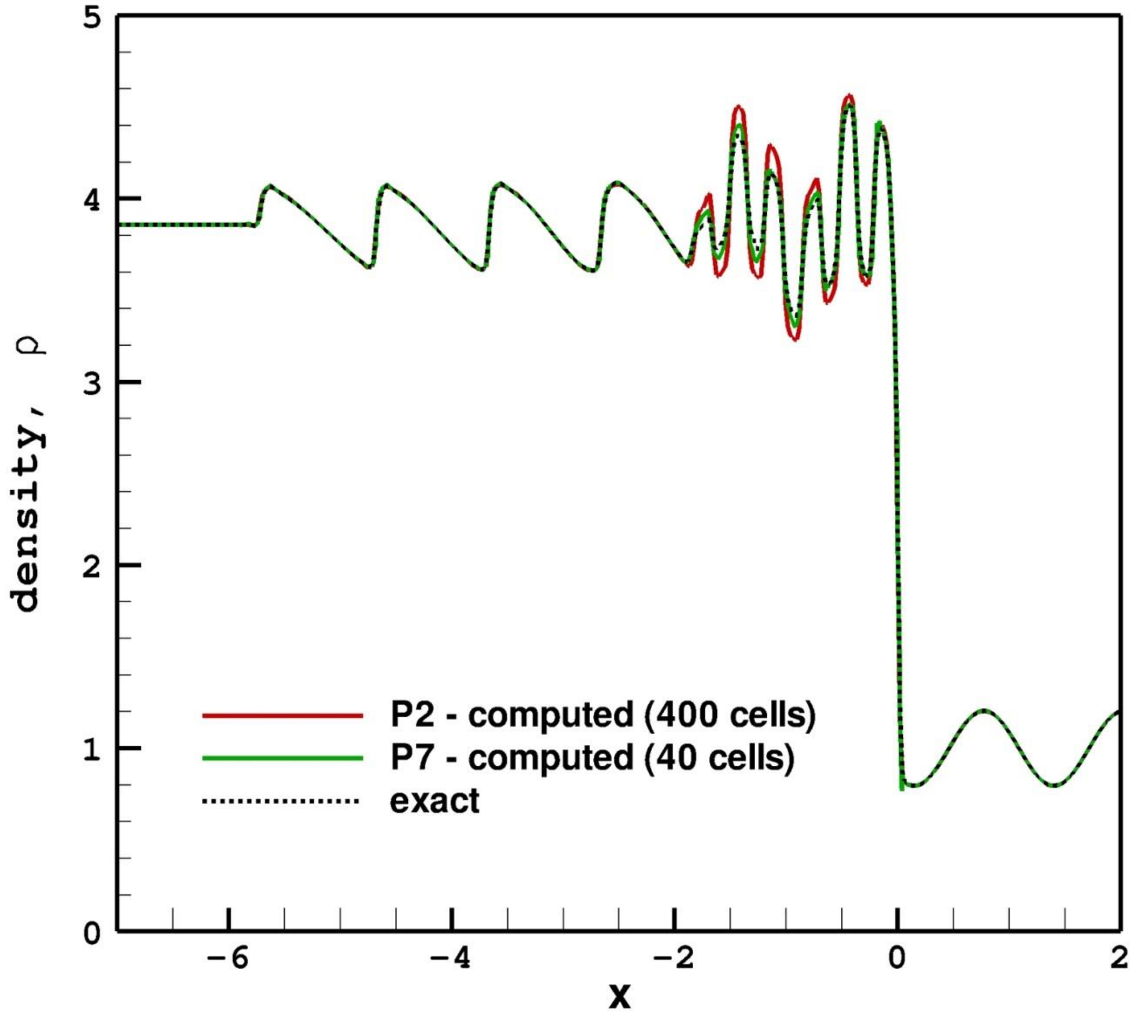

M=3, β=30 oblique shock reflection

Convergence to the design order of accuracy has been achieved

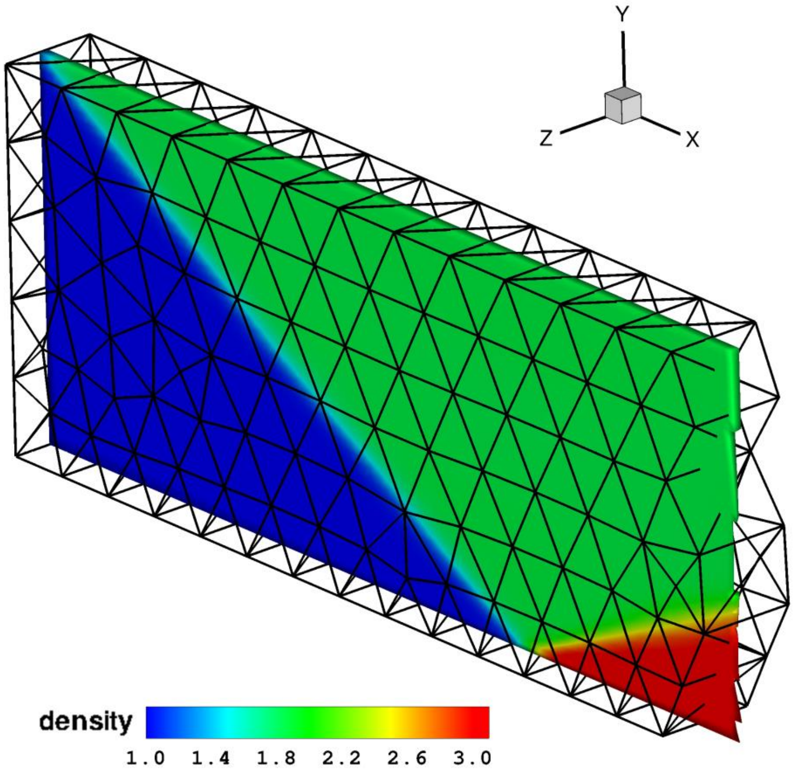

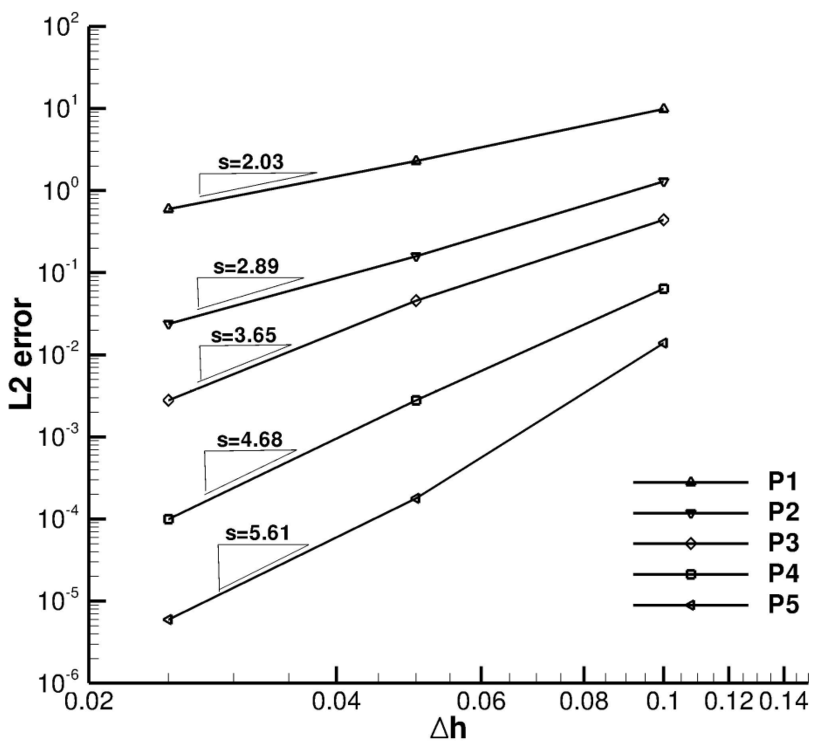

NACA-0012 airfoil at M = 0.8, $\alpha = 1.25^o$

P4 numerical solution P2 surface elements

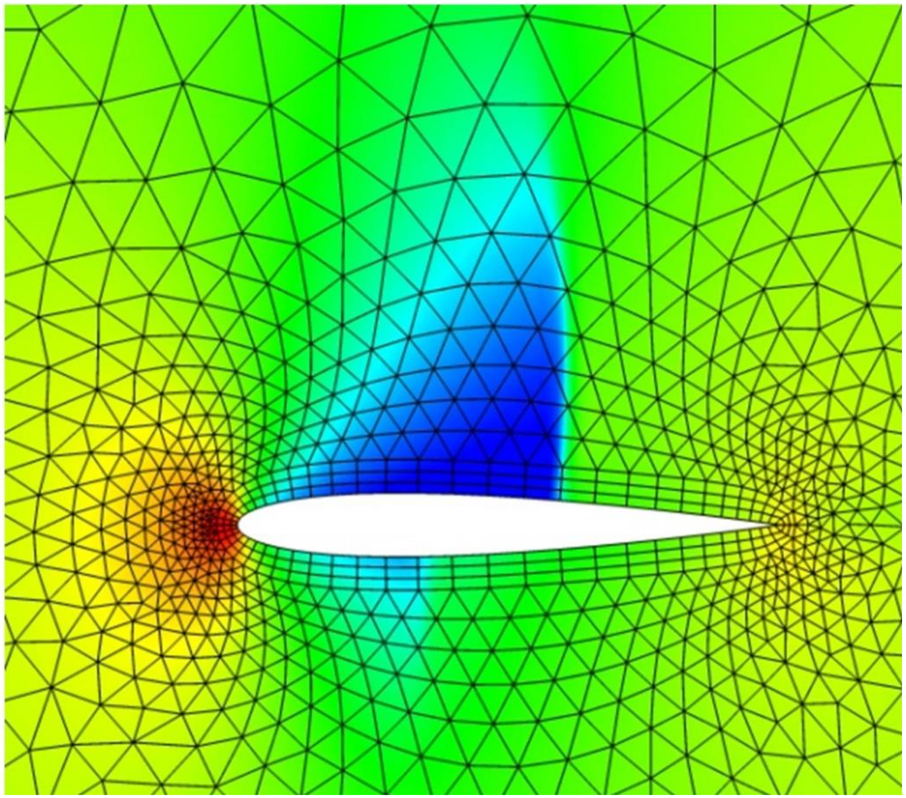

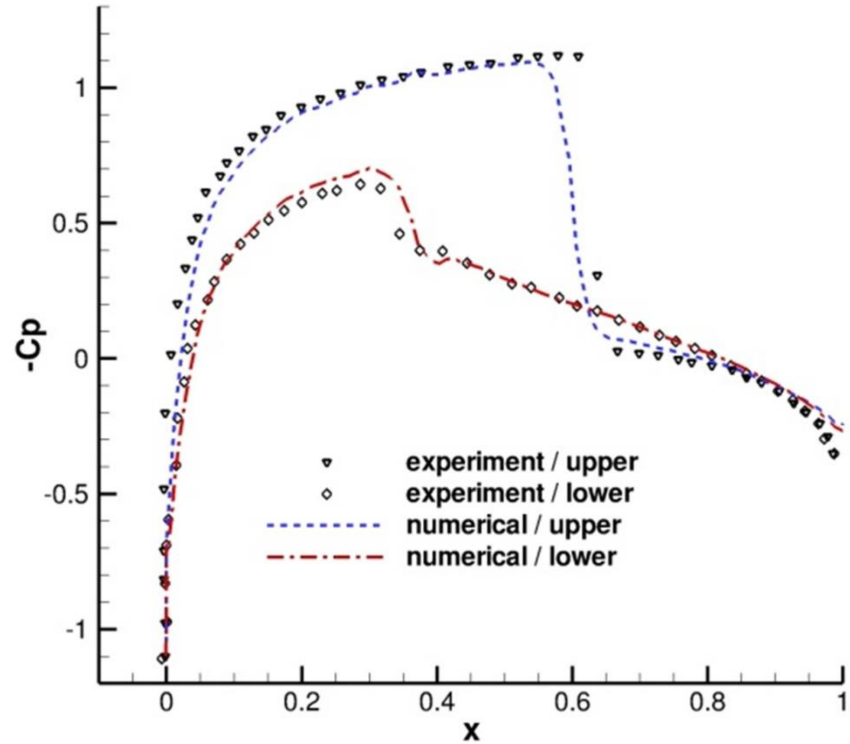

Flow at M = 3 in a tunnel with a step

P1
Filtered
h = 1/80

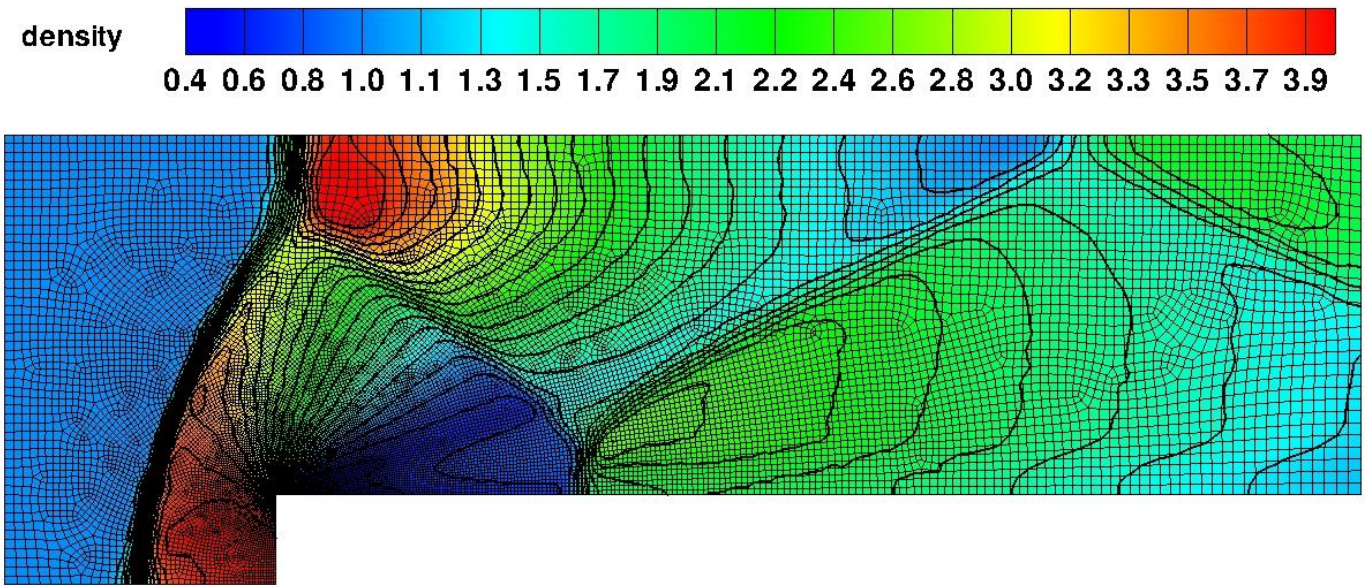

P1
TVB limiter
H = 1/120

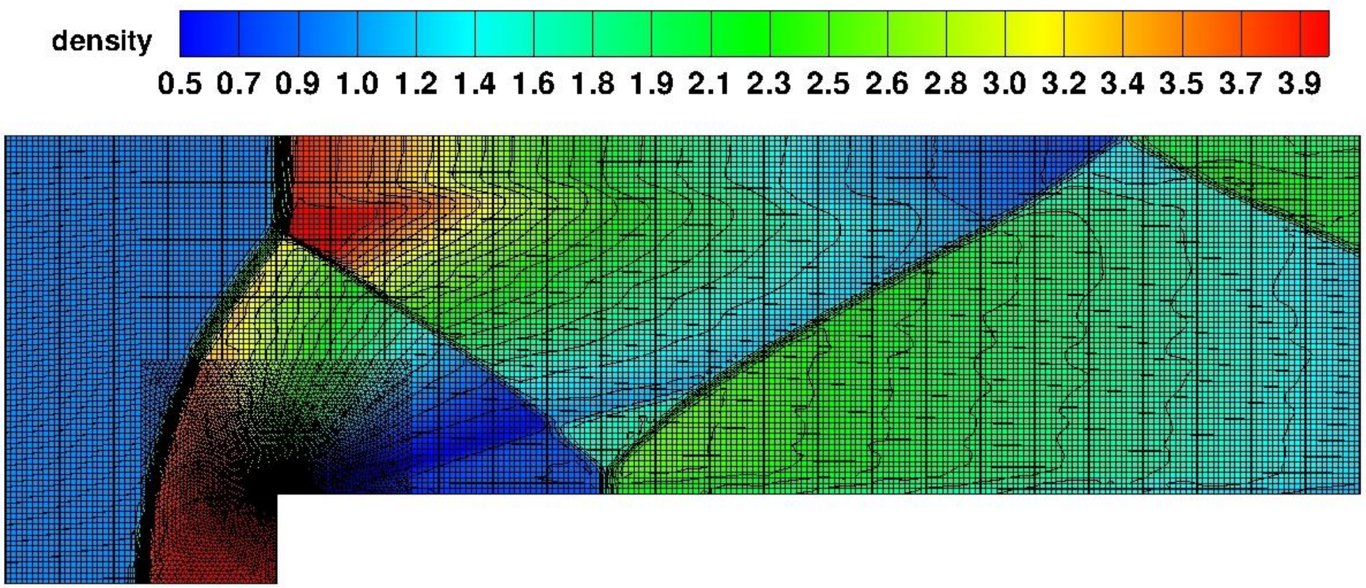

Flow at M = 3 in a tunnel with a step

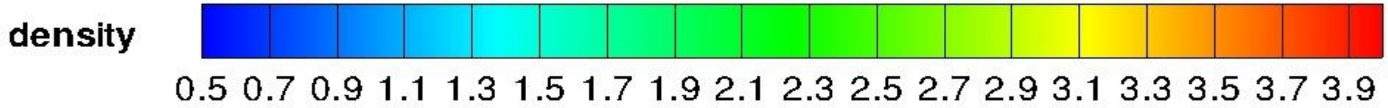

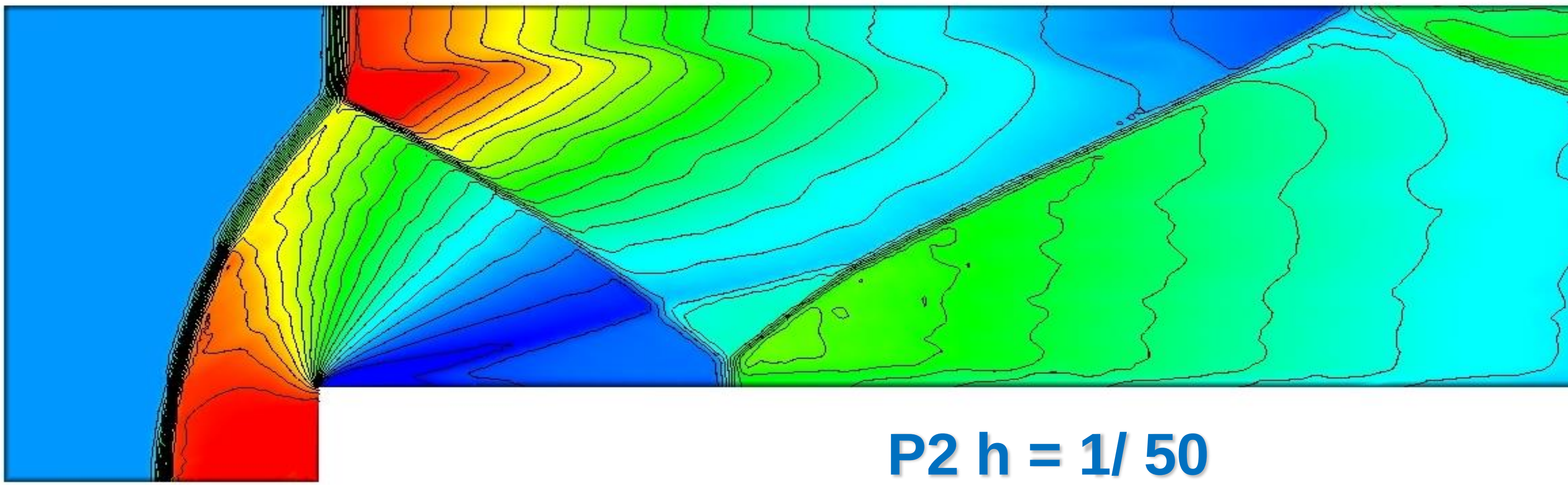

P2 h = 1/ 50

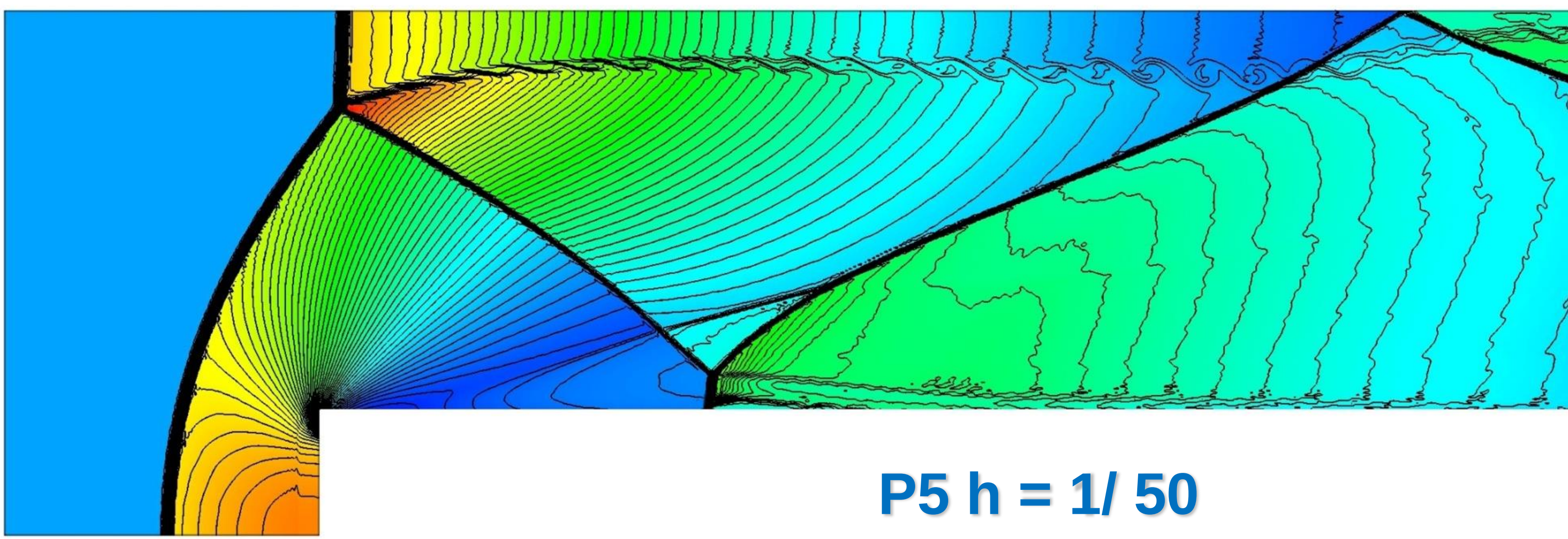

P5 h = 1/ 50

Flow at M = 3 in a tunnel with a step

P1 adaptive
h = 1/ 640
at shocks and slip lines

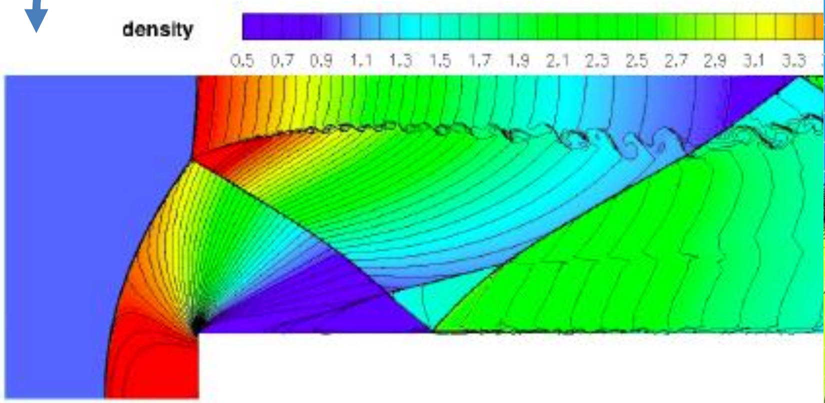

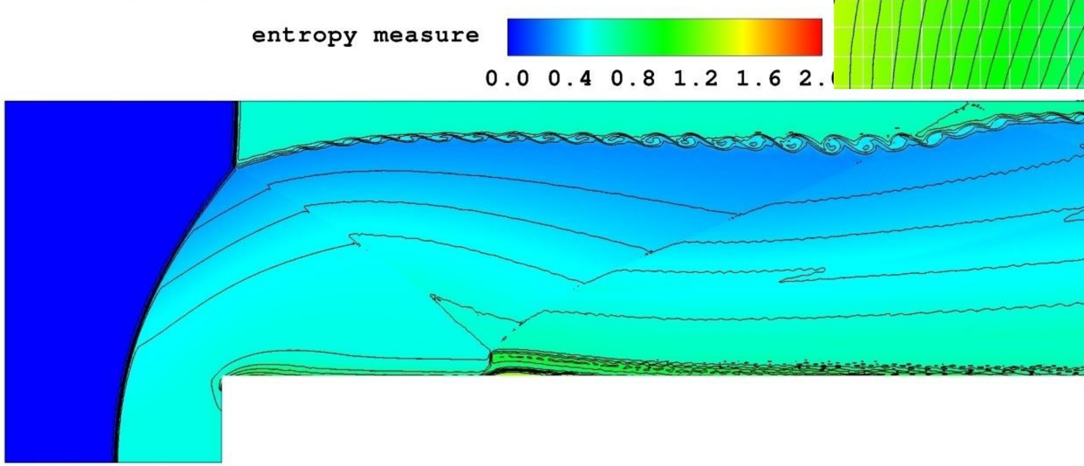

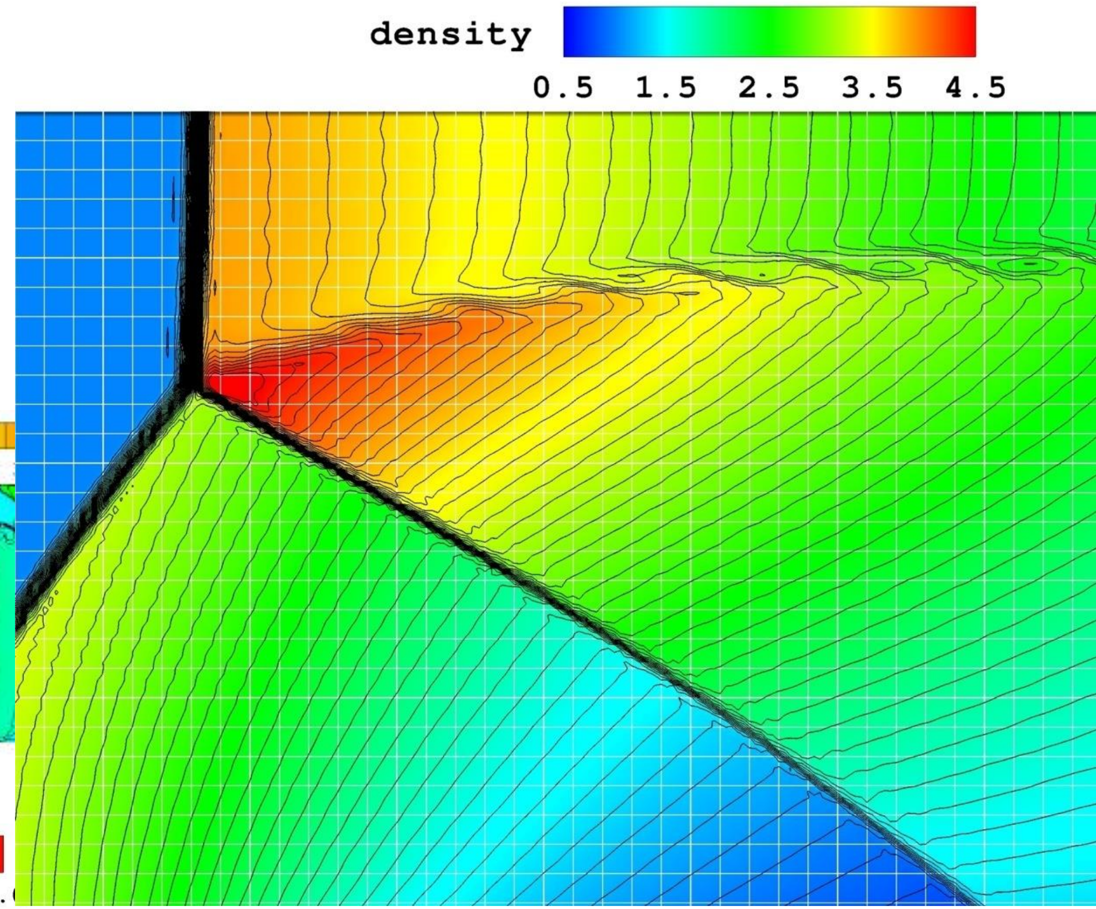

P5 h = 1/ 50

Reflection of a M=2 shock from a wavy

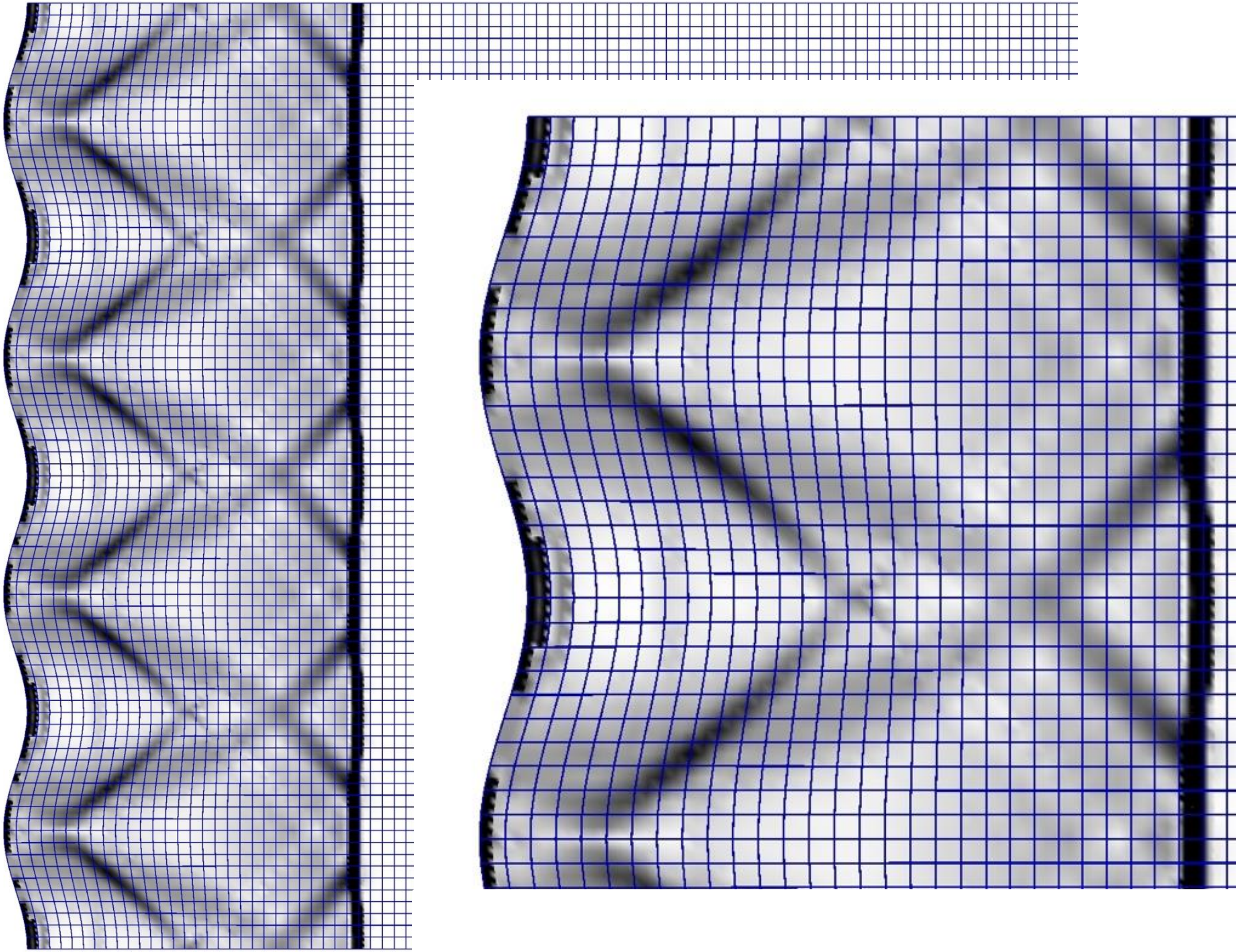

Reflection of a M=2 shock from a wavy

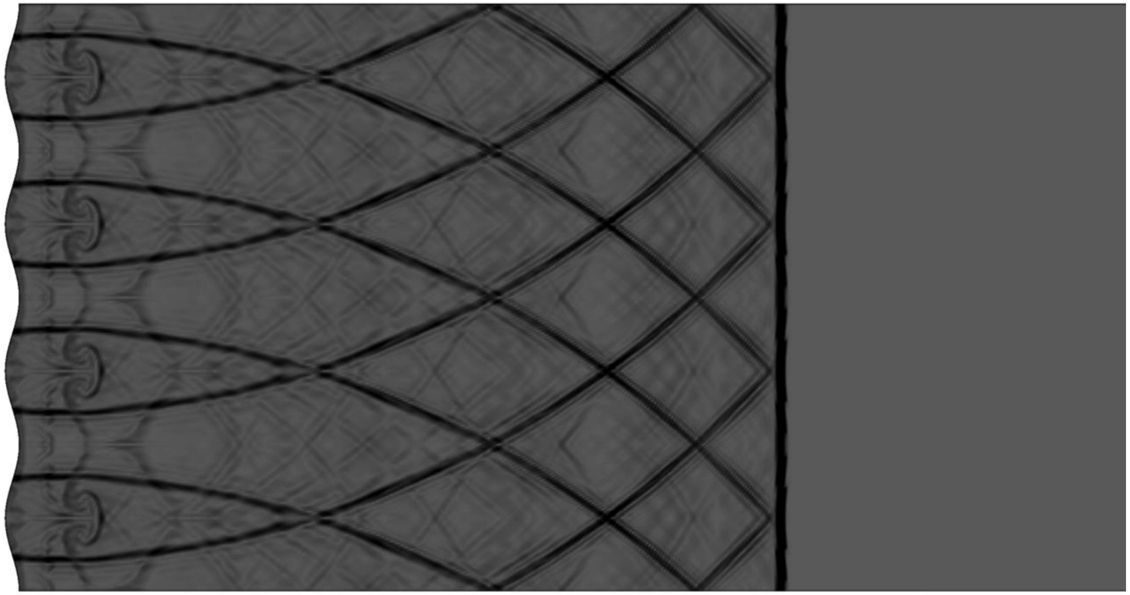

Computed density gradient numerical schlieren

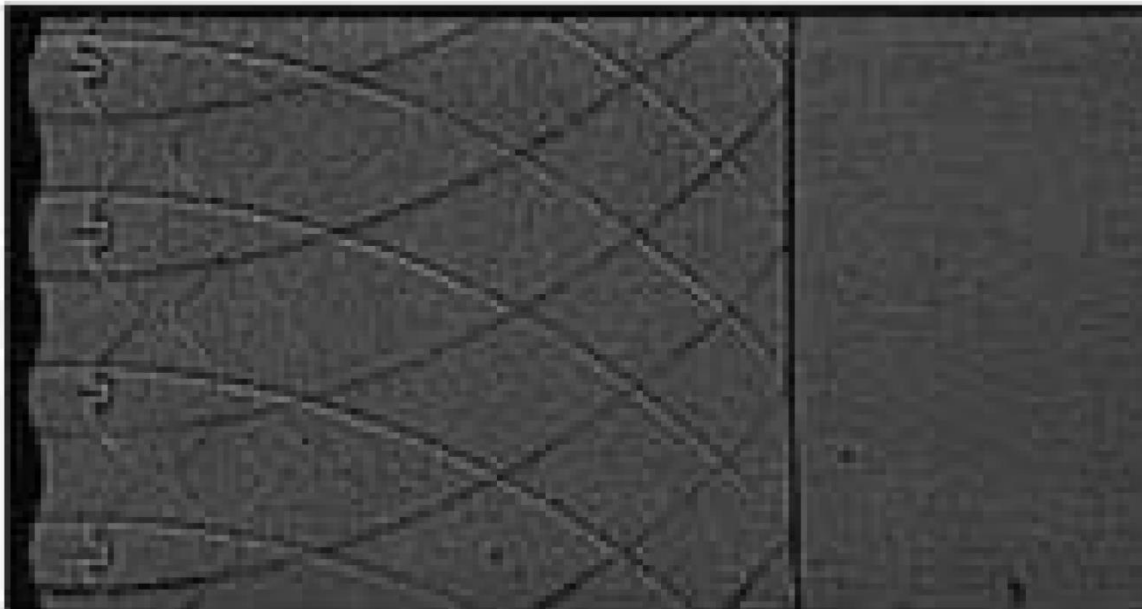

Experimental sclieren

Reflection of a M=2 shock from a wavy wall

density t = 350 ❍*s*

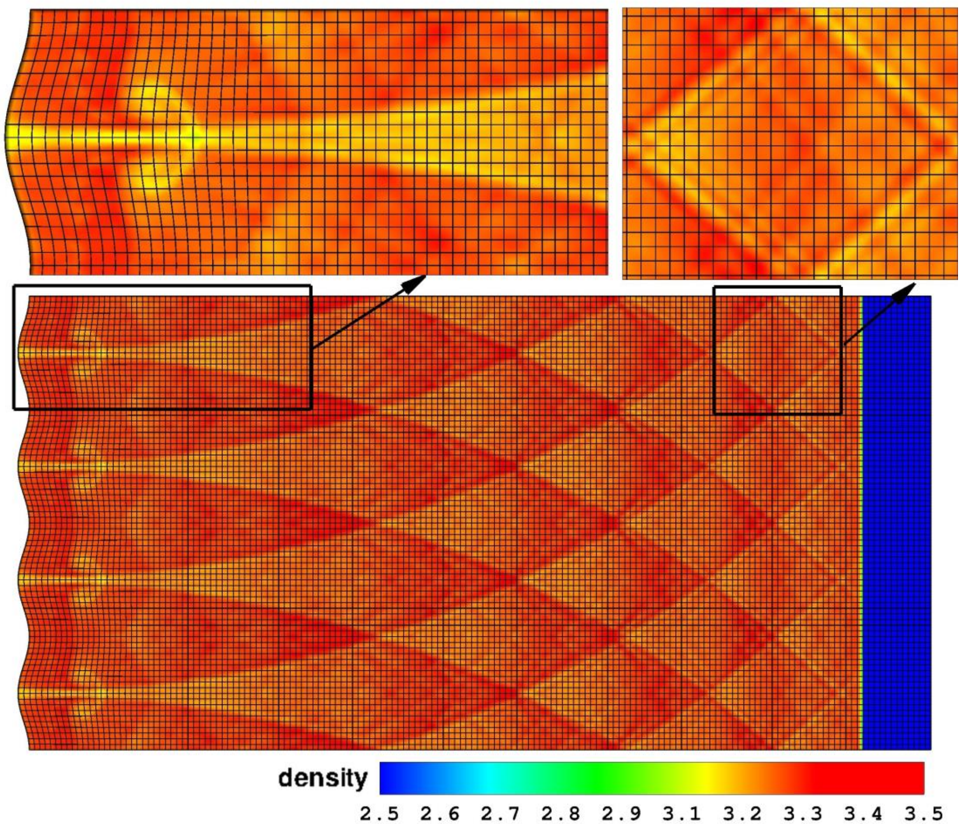

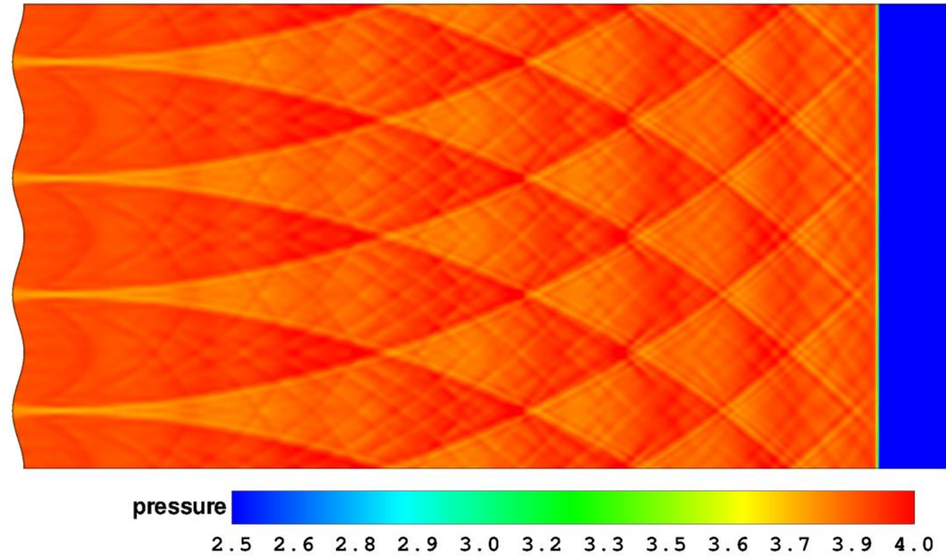

density dradient

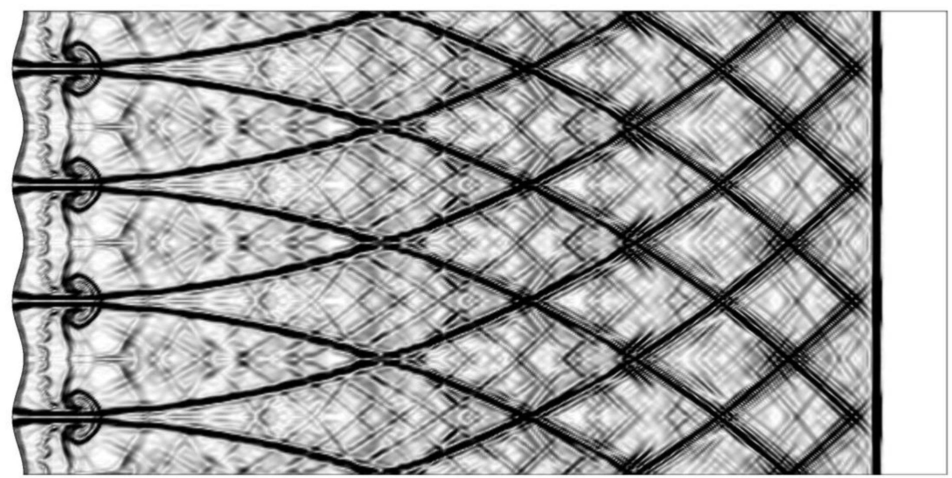

Transonic flow at M = 0.8, ONERA M6 wing
P1 numerical solution on fine hexahedral mesh

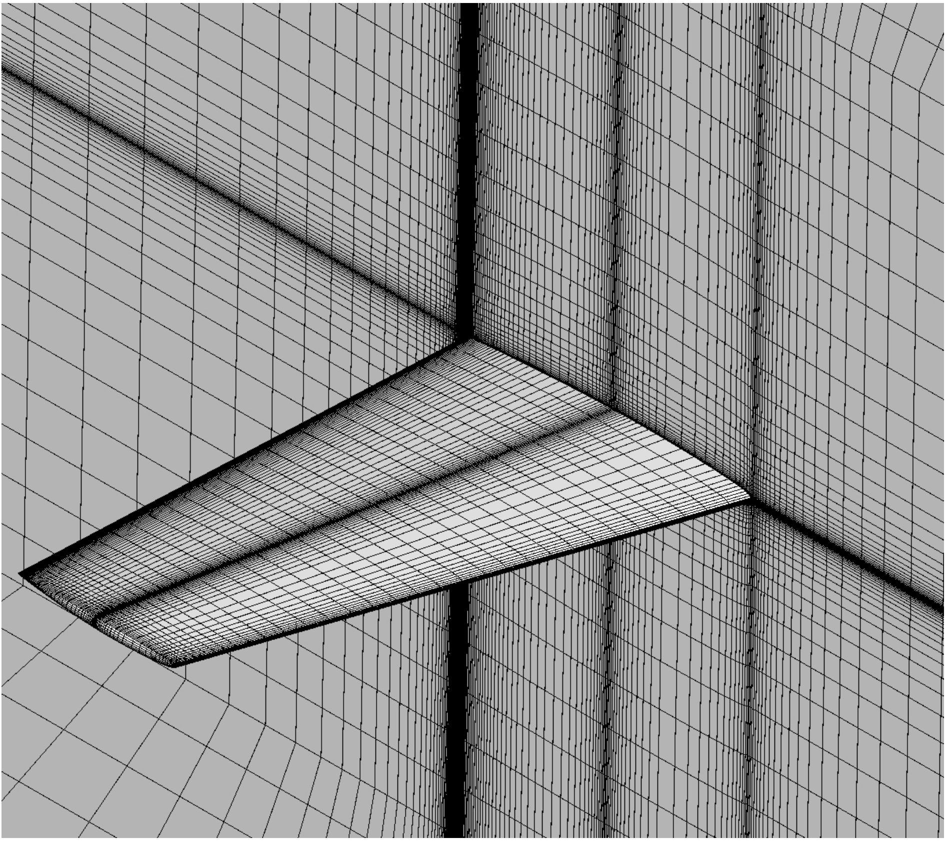

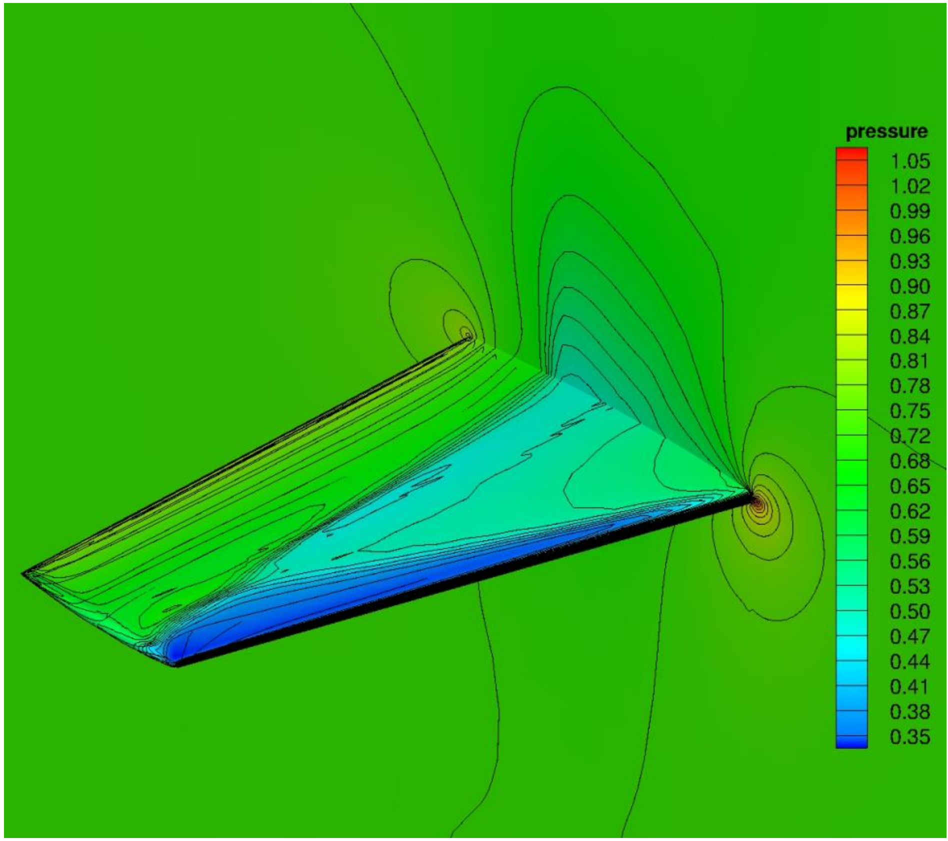

Transonic flow at M = 0.8, ONERA M6 wing
P1 numerical solution with AMR

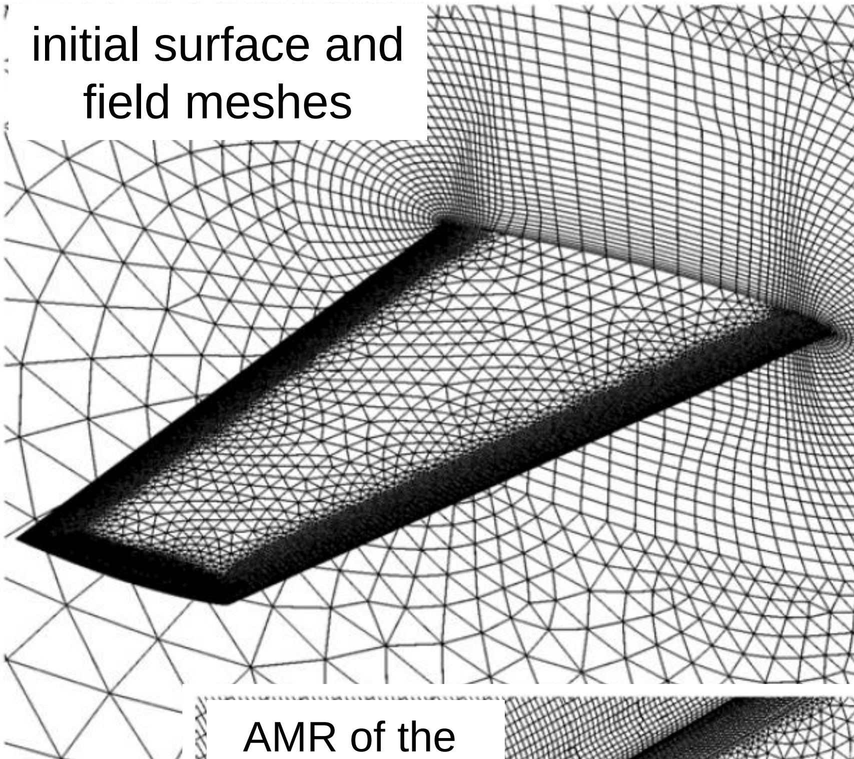

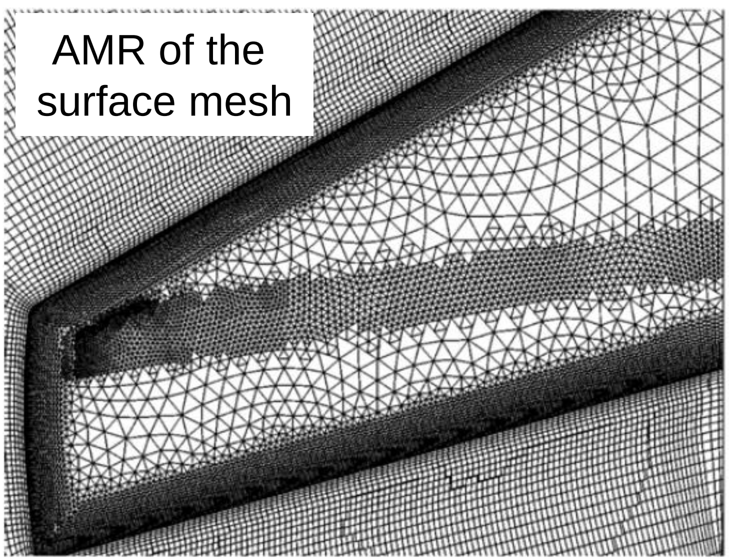

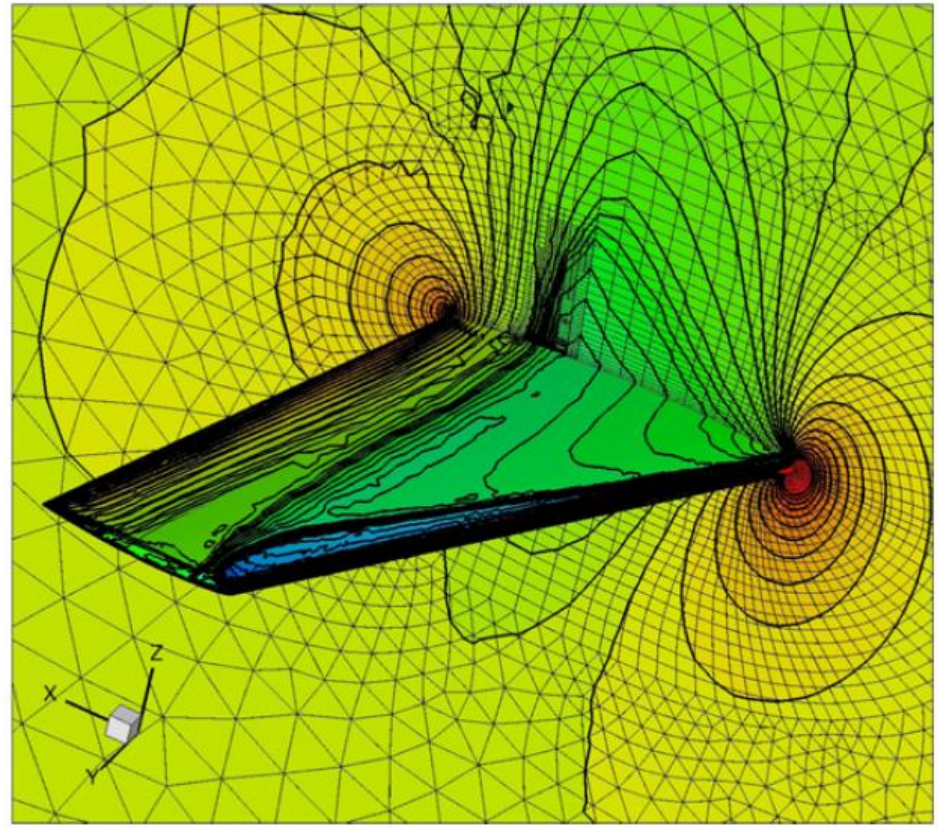

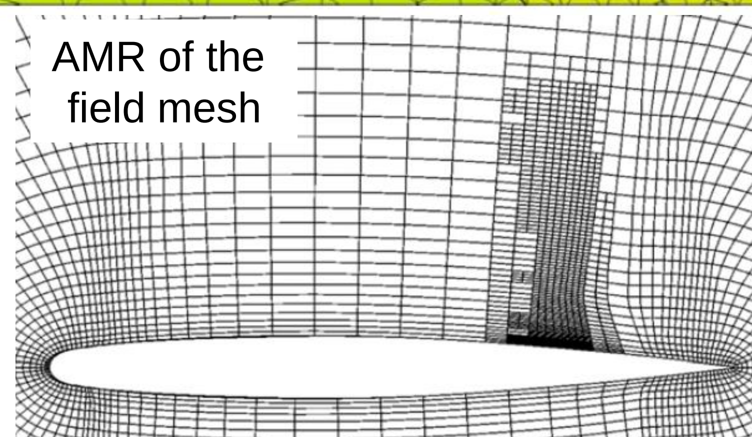

ONERA M6 wing P1 solution at M = 0.8

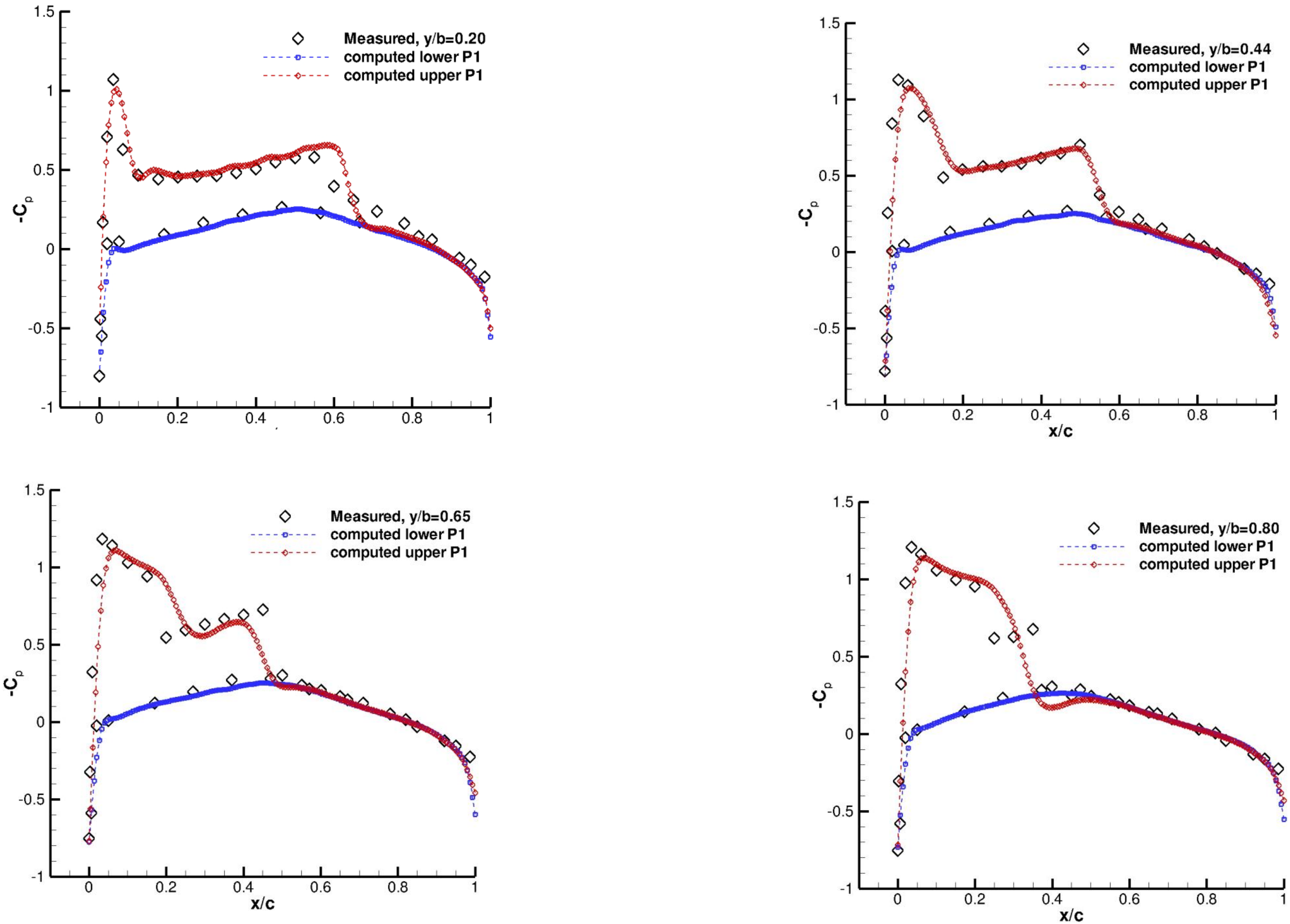

ONERA M6 wing M = 0.8, P3 sub-cell shock capturing

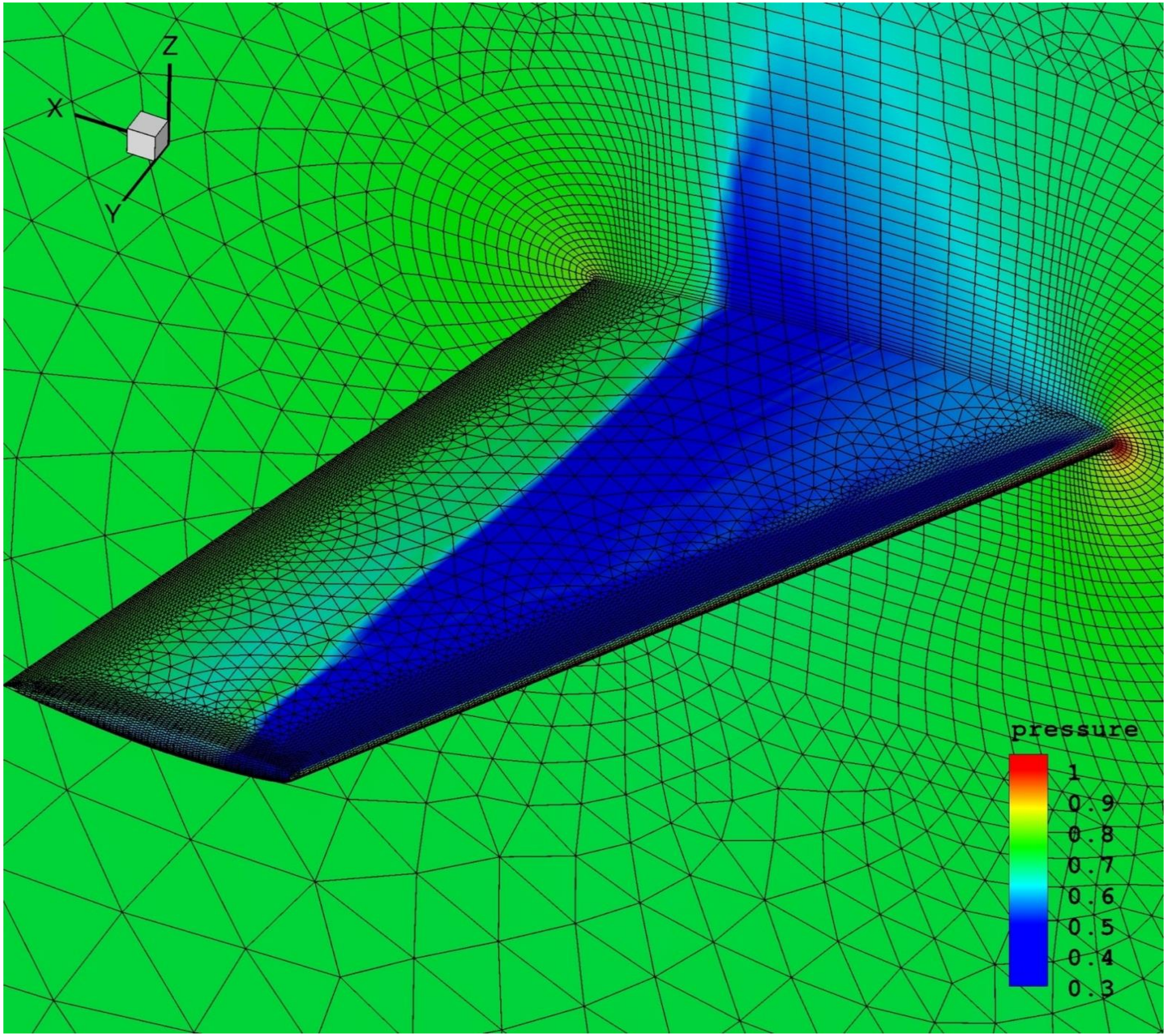

ONERA M6 wing P3 solution at M = 0.8

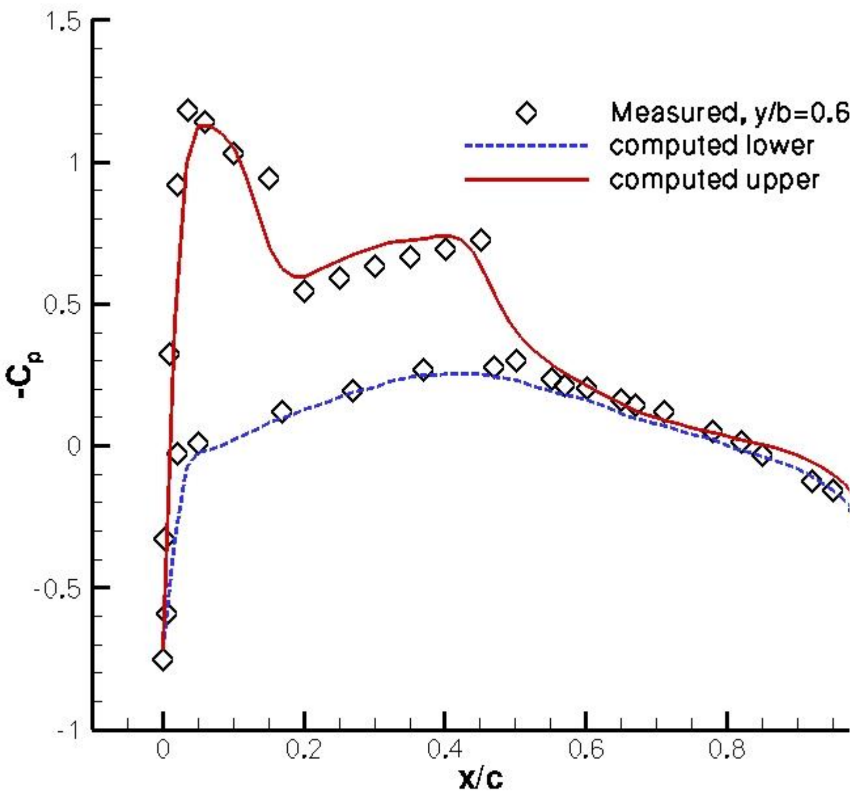

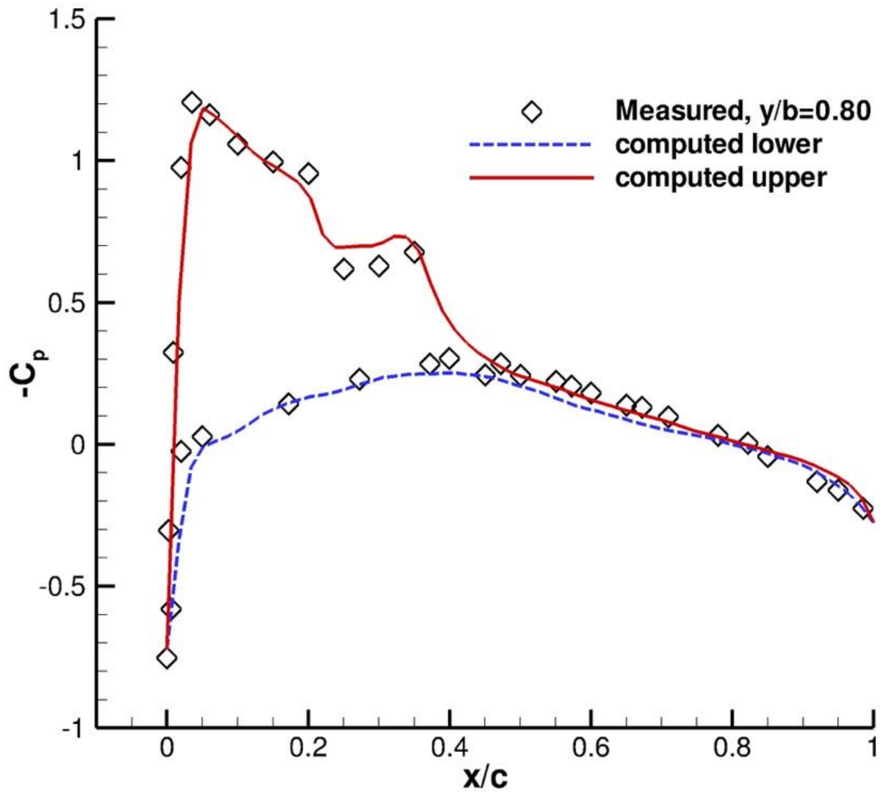

ONERA M6 wing M = 0.8, P4-P5 shock capturing

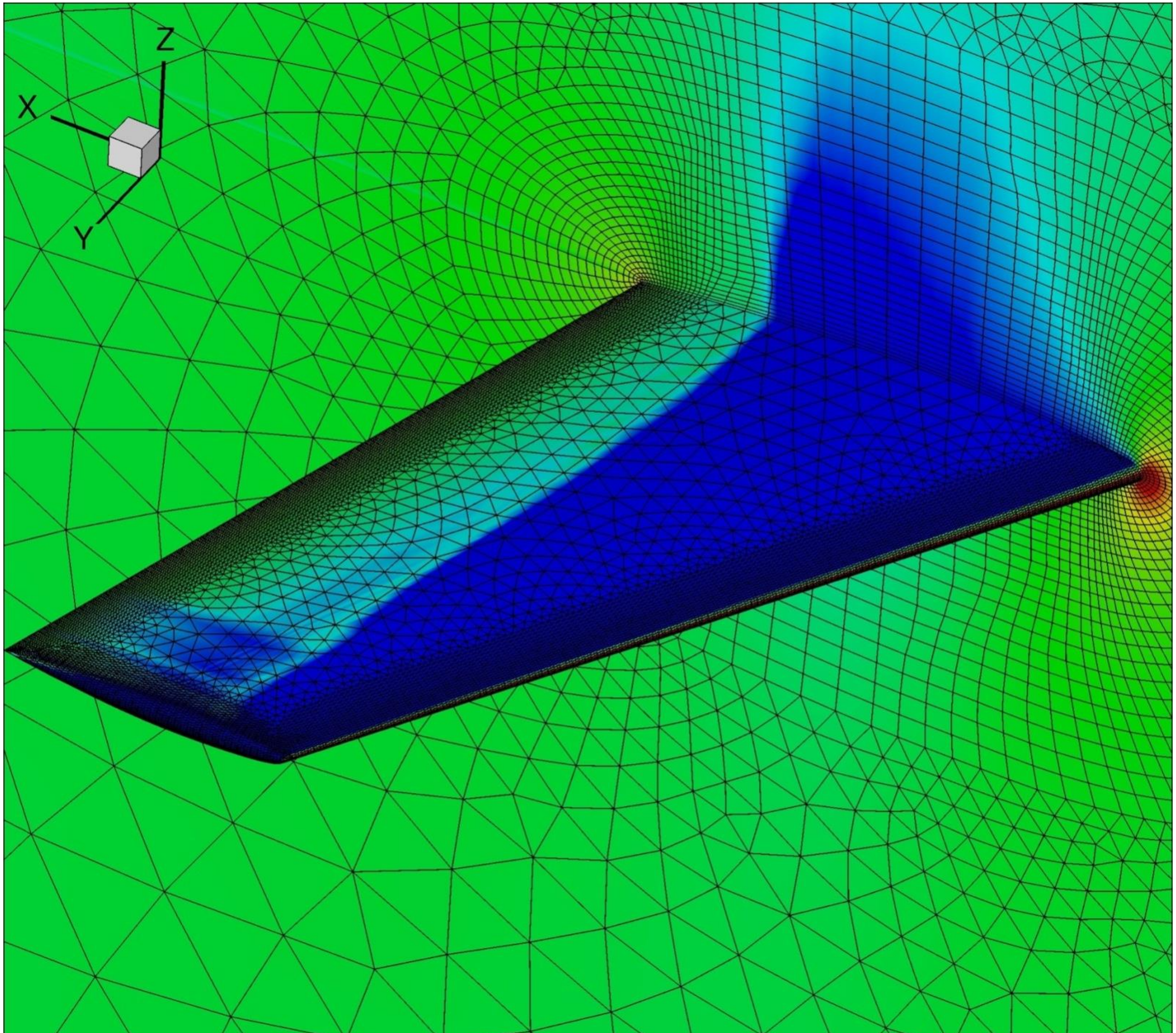

h/p adaptivity for chemically reacting flow at M = 8

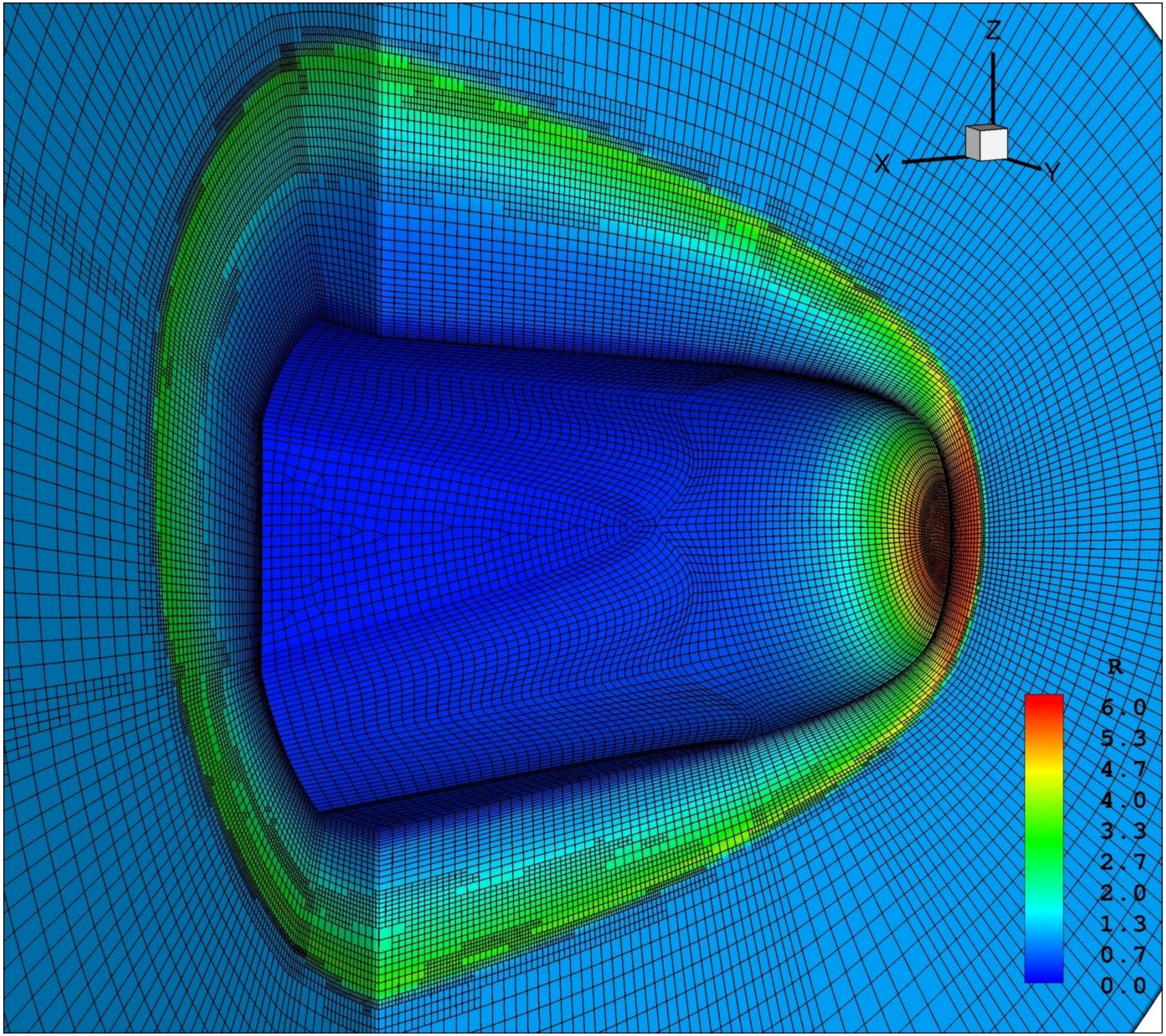

Chemically reacting flow at M = 8

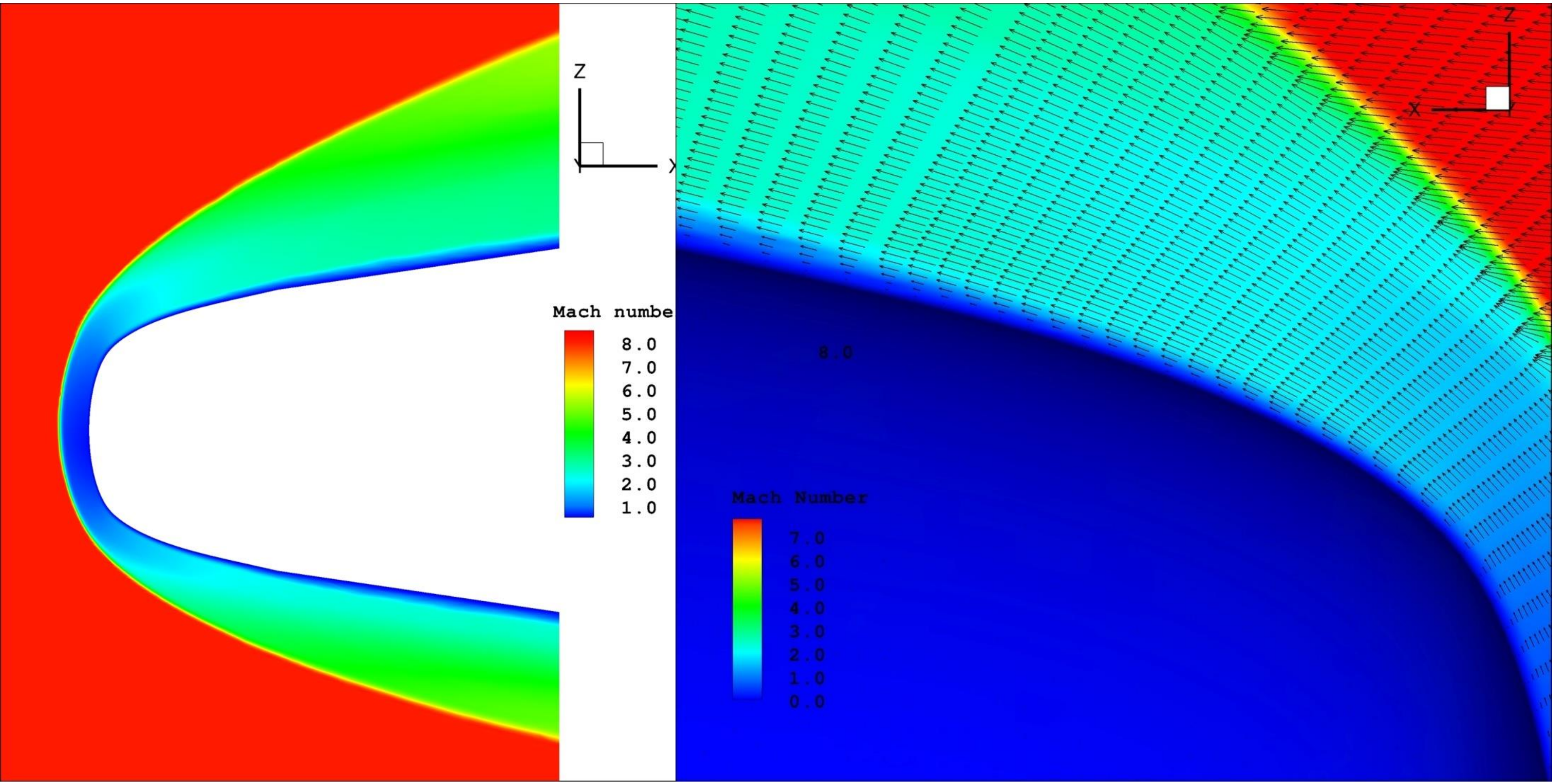

Chemically reacting flow at M = 8

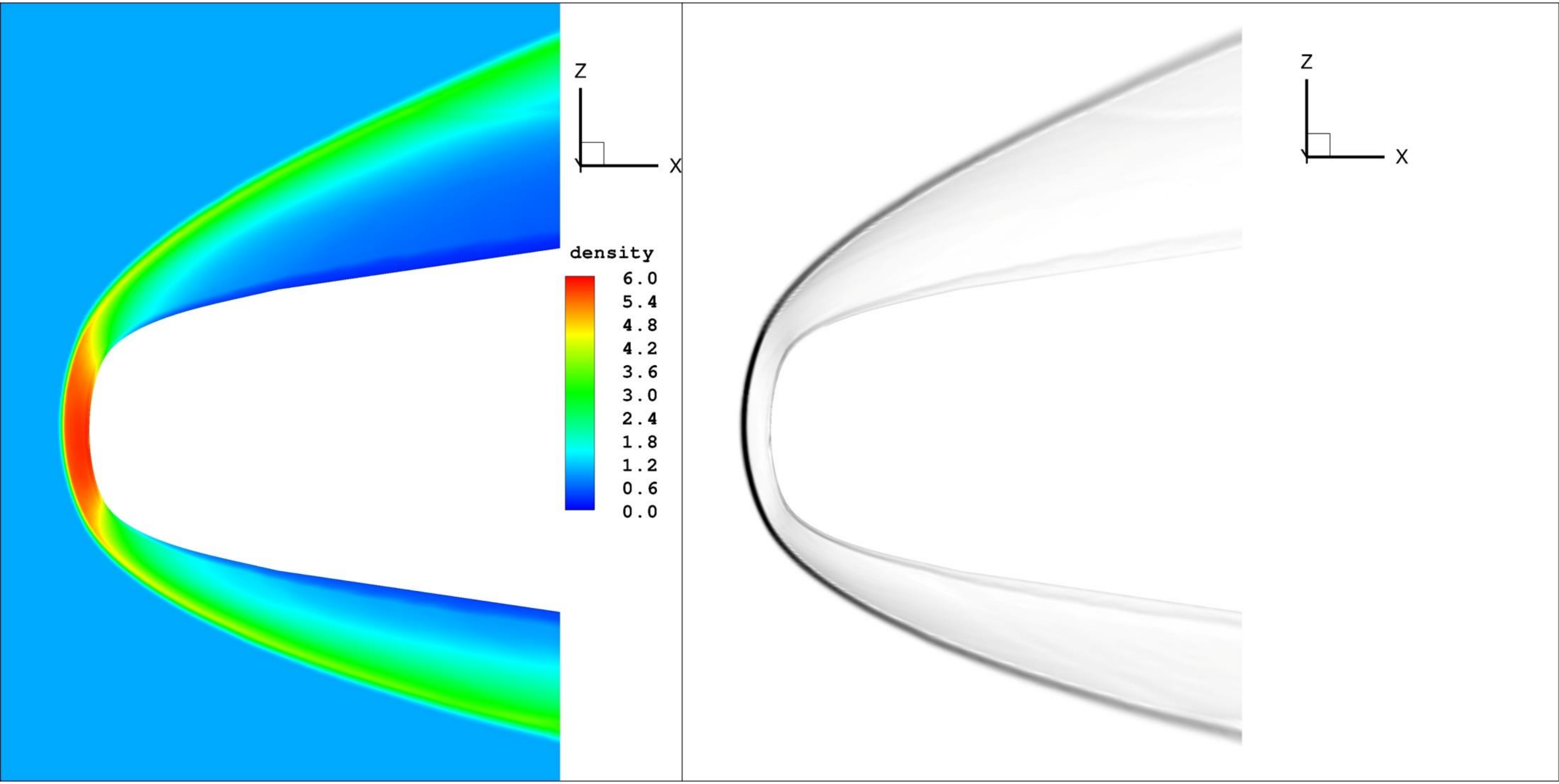

h/p adaptivity for chemically reacting flow at M = 8

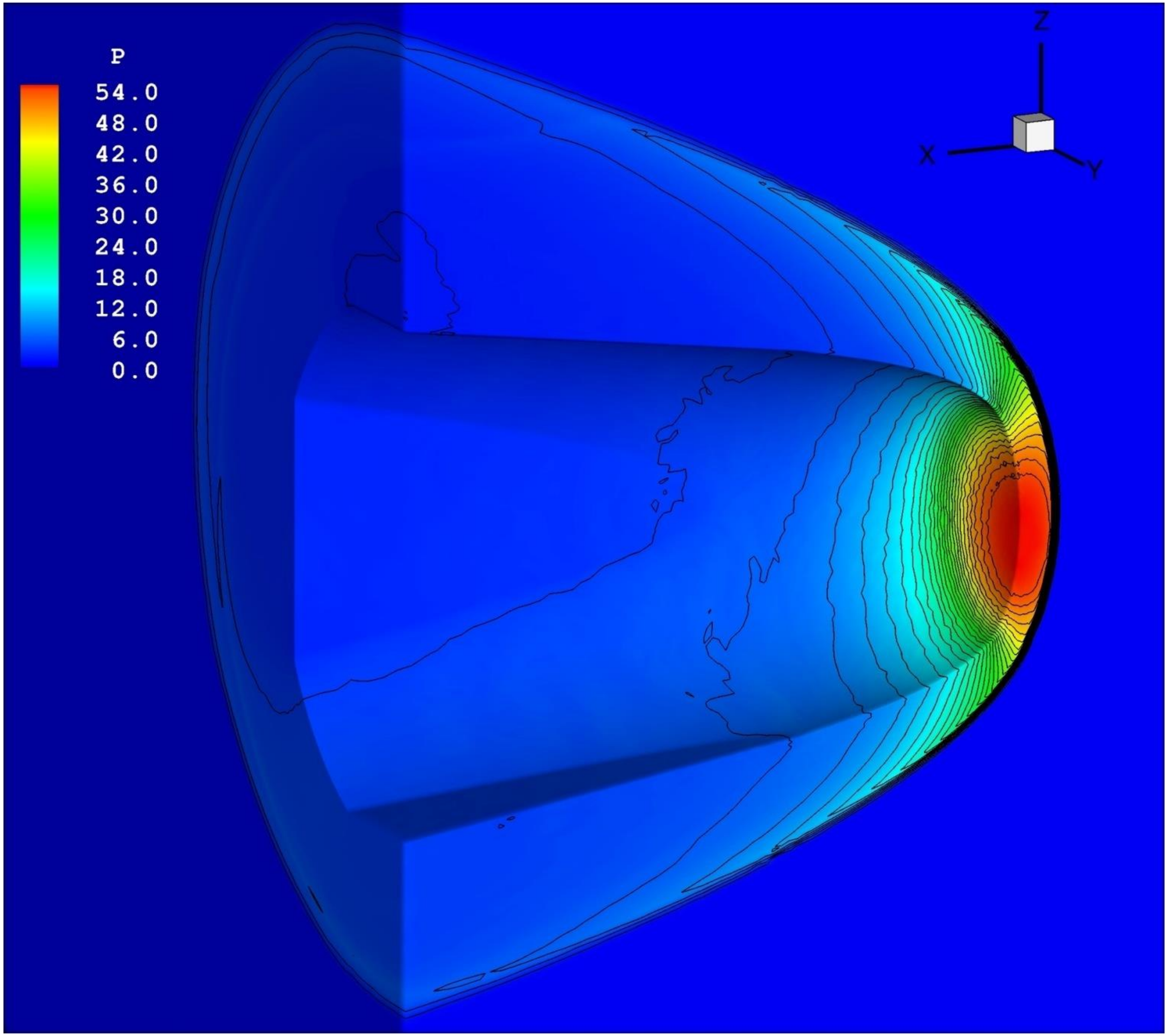

Chemically reacting flow at M = 8

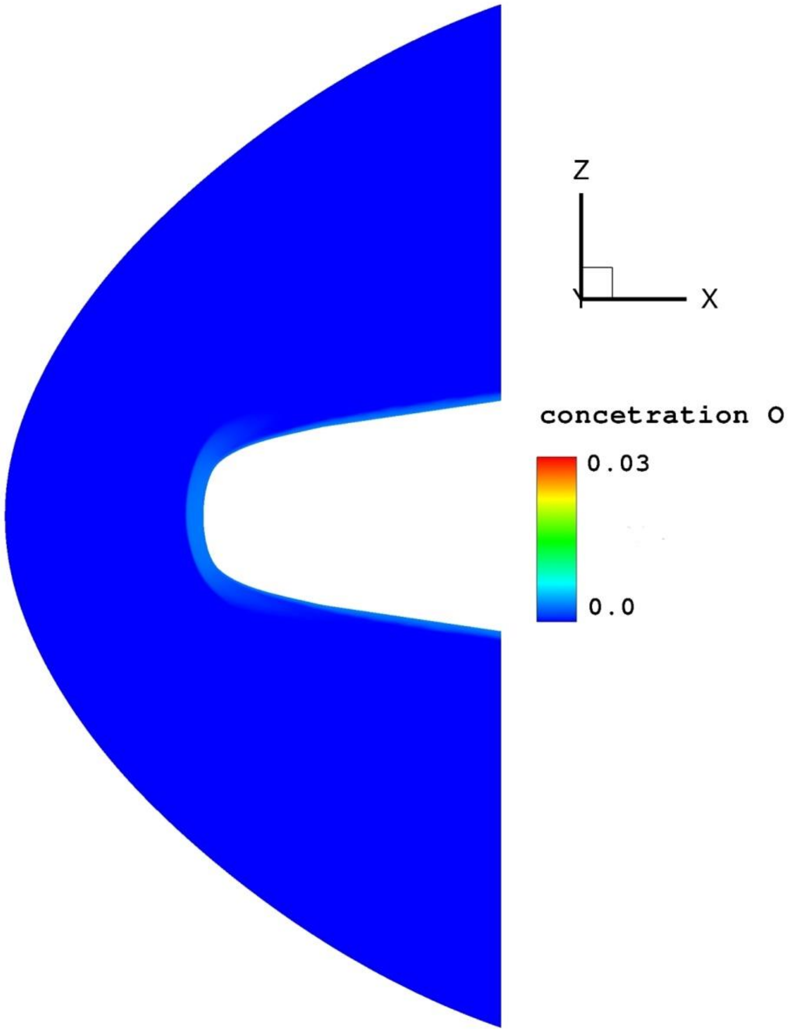

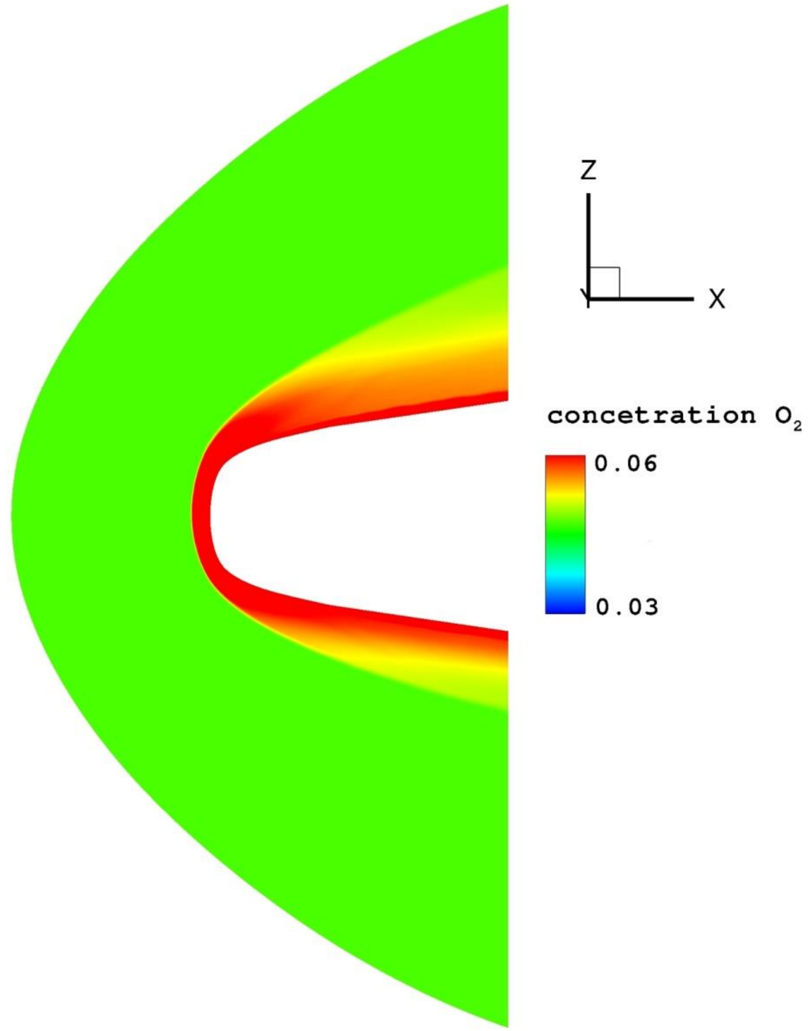

Chemically reacting flow at M = 8

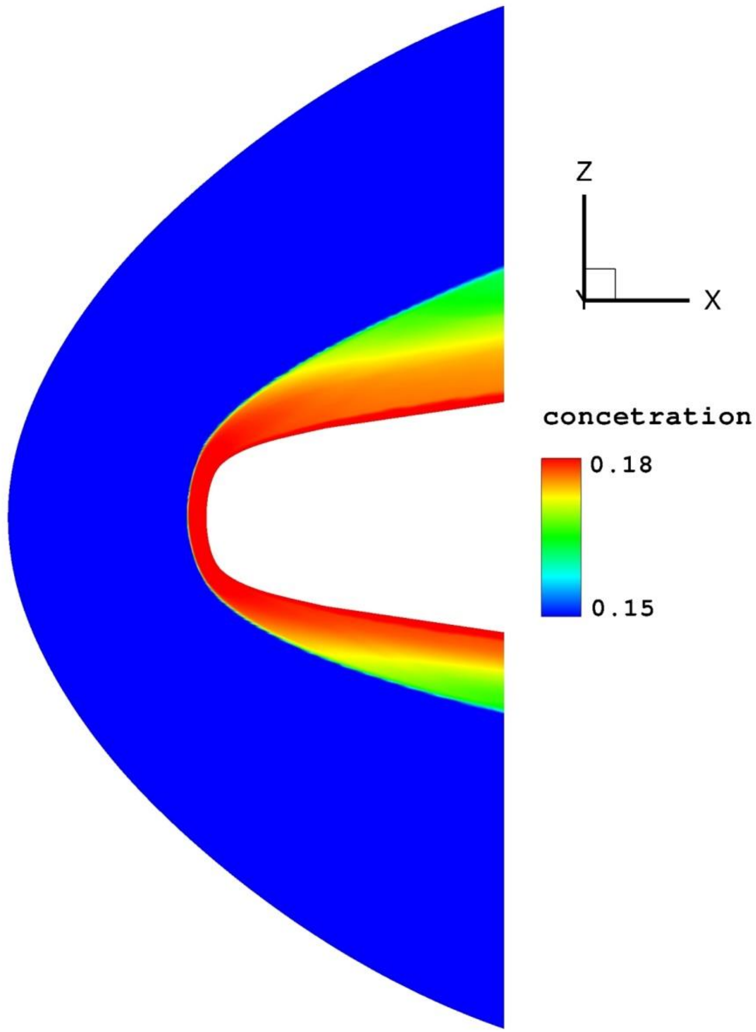

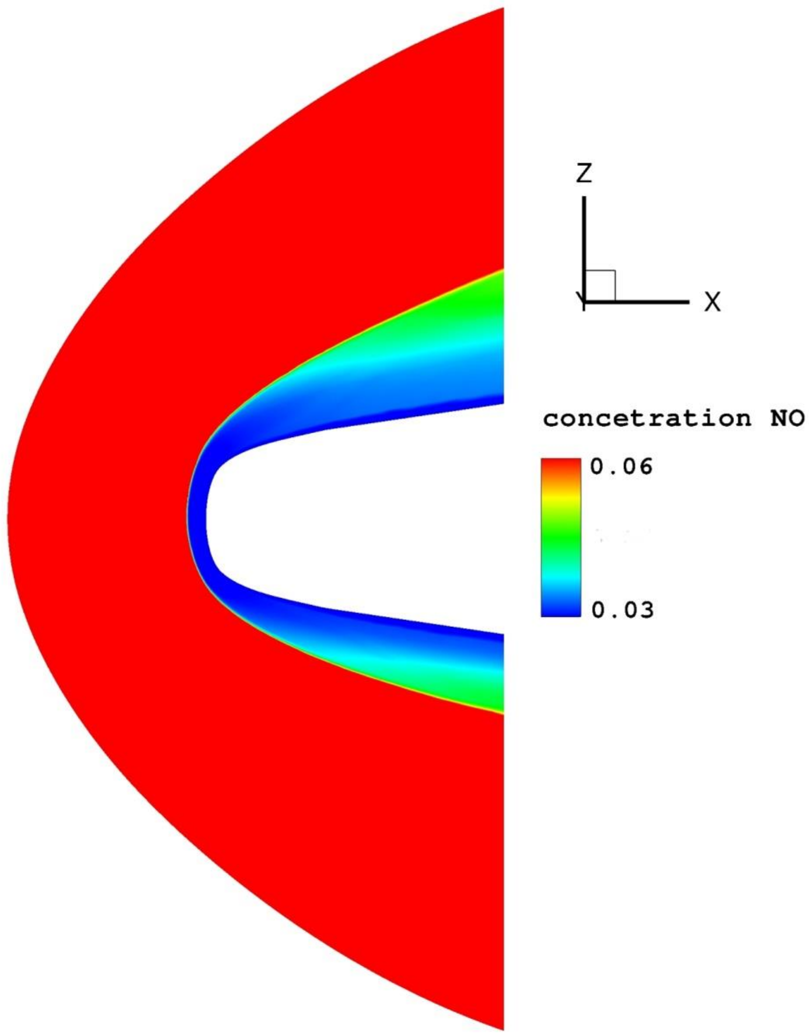

Outlook for high order DG methods

- Application of p-adaptivity, and AMR for smooth features and discontinuties was demonstrated

- A unified filtering approach for high order DG discretizations in unstructured three-dimensional meshes was developed. Filtering is applied as a post processing stage and it is suitable for both implicit and explicit time marching

- Computationally intensive hierarchical limiting of higher order DG discretizations is not required and sub-cell discontinuity resolution is achieved. Benefits from filtering higher order expansions were found

- Combined dynamic h/p refinement can be applied for problems with discontinuities and embedded smooth but complex flow features to increase efficiency of DG discretizations without compromising numerical accuracy

- Furthered enhancements are expected from the isogeometric approach and its implementation to complex fluid structure interaction problems and other disciplines